

207

Optimizing Interplanetary Trajectories With Deep Space
Maneuvers

by

John 'Fuzz' Navagh

B.S.M.E. June 1991, State University of New York at Buffalo

Submitted to the Faculty of
The School of Engineering and Applied Science
of
The George Washington University
in partial fulfillment of the requirements for the degree of
Master of Science

July 1993

Thesis directed by
Dr. Robert H. Tolson
Professor of Engineering and Applied Sciences
The George Washington University

This research was conducted at the NASA Langley Research Center

I. Abstract

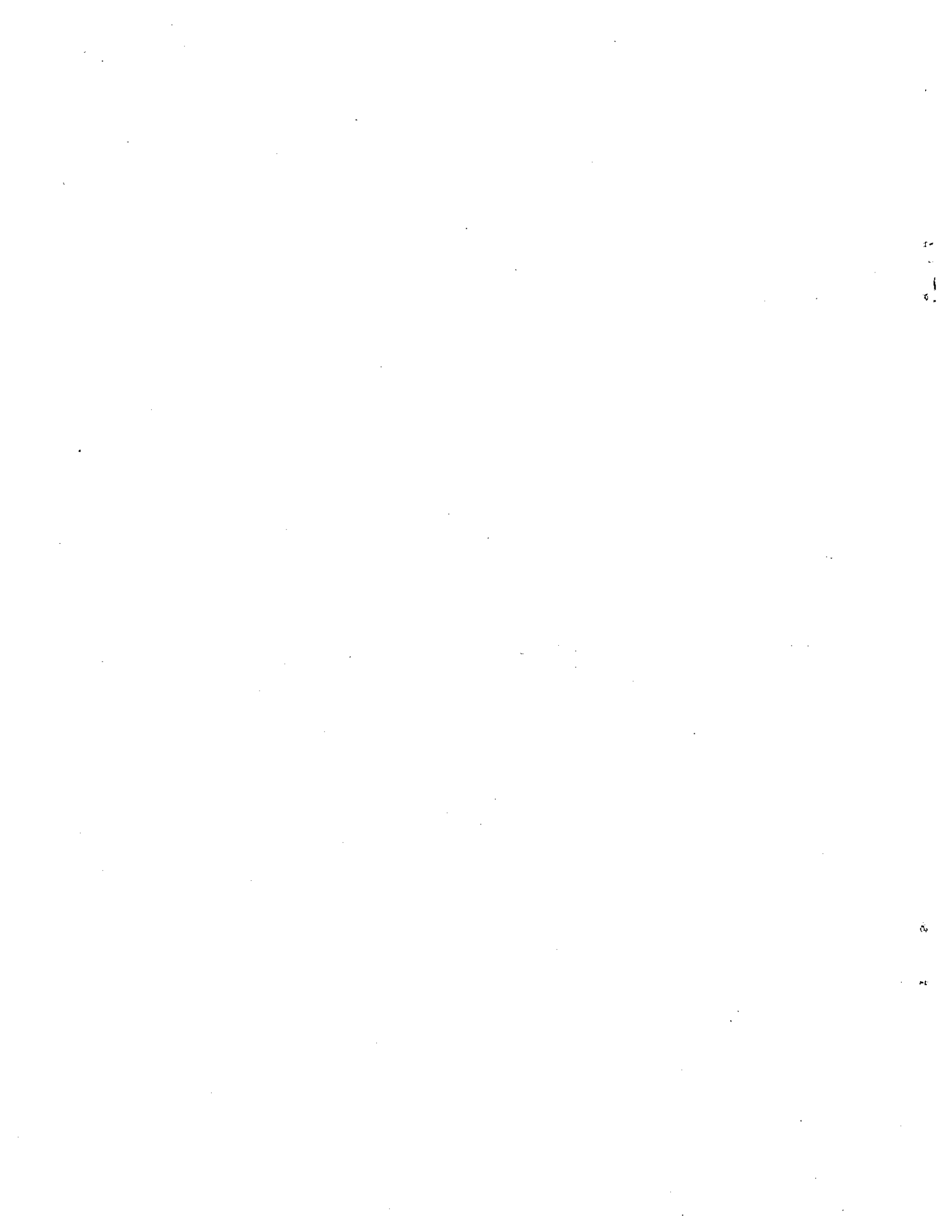
Analysis of interplanetary trajectories is a crucial area for both manned and unmanned missions of the Space Exploration Initiative. A deep space maneuver (DSM) can improve a trajectory in much the same way as a planetary swingby. However, instead of using a gravitational field to alter the trajectory, the on-board propulsion system of the spacecraft is used when the vehicle is not near a planet. There are occasions (broken plane maneuvers are one example) where the advantages gained at the endpoints of the trajectory outweigh the cost of the DSM. The purpose of this study is to develop an algorithm to determine where and when to use deep space maneuvers to reduce the cost of a trajectory. The approach taken to solve this problem uses primer vector theory in combination with a non-linear optimizing program. Primer vector theory applies the calculus of variations to the trajectory problem in order to minimize ΔV . A set of necessary conditions on a Lagrange multiplier called the primer vector arises from the analysis, and this primer vector indicates whether a deep space maneuver will be beneficial. Deep space maneuvers are applied to a round trip mission to Mars to determine their effect on the launch opportunities. Other studies which were performed include cycler trajectories and Mars mission abort scenarios. It was found that the software developed was able to quickly locate DSM's which lower the total ΔV on these trajectories.



II. Acknowledgments

There are many people that deserve thanks for the help they have provided to me during the course of this research. First of all, I would like to thank my advisor, Dr. Tolson, for providing most of the research material. Also, his quick answers to questions which I tried to answer myself for weeks at a time kept me on track throughout the duration of this project. The most memorable piece of advice I received from Dr. Tolson was, "Always check your assumptions." I have found this to be sound advice for engineering applications as well as many other situations in everyday life.

I would also like to thank people in the Vehicle Analysis Branch, including, but not limited to Prasun Desai, Dick Powell, and Scott Striepe. It was their knowledge of orbital mechanics and of IPREP which provided the driving motivation behind this research. I would also like to thank Perry Kent of the Martin Marietta Corporation for his many answers to questions about the inner workings of IPREP. Finally, I would like to thank my friends and family, especially my parents, for their support of all my efforts.



III. Table of Contents

I. Abstract	i
II. Acknowledgments	ii
III. Table of Contents	iii
IV. Lists of Tables and Figures	v
V. Nomenclature	iv
1. Introduction	
Background	1
Thesis Organization	3
2. Analysis	
Description of IPREP	4
Primer Vector Theory	7
Approximating the Location of a Deep Space Maneuver	12
Finding Deep Space Maneuvers on Trajectories With Swingby's	14
3. Software Developed	
Integration into IPREP	15
Optimizer	16
4. Results	
Cycler Trajectory Analysis	19
Launch Window Analysis	21
Abort Mission Analysis	22
5. Conclusions	24
6. Recommendations for Future Work	26
7. References	27
8. Tables	30
9. Figures	36

10. Appendix49

IV. List of Tables and Figures

Table 4.1:	Comparison of BPLANE Code and PRIMER Code for Cycler Trajectory from Reference 10	30
Table 4.2:	Comparison Between BPLANE Code and PRIMER Code for Cycler Trajectory When a DSM is Allowed on Each Leg	31
Table 4.3:	Vehicle and Mission Parameters for Round Trip Mars Mission Launch Window Analysis	33
Table 4.4:	Vehicle and Mission Parameters for Nominal Mars Mission Abort Analysis	34
Table 4.5.1	Comparison Between Nominal and Abort Trajectories for 2020 Mars Mission	35
Table 4.5.2	Comparison Between Nominal and Abort Trajectories for 2020 Mars Mission	35
Figure 1.1:	Rendezvous Between Points A and B	36
Figure 1.2:	Representative Optimal Primer Magnitude History	37
Figure 1.3:	Representative Optimal Primer Magnitude History	37
Figure 1.4:	Representative Non-Optimal Primer Magnitude History	38
Figure 1.5:	Representative Non-Optimal Primer Magnitude History	38
Figure 2.1:	Perturbations from the Nominal Trajectory	39
Figure 4.1:	Primer Magnitude History for Leg 6 in Table 4.1	40
Figure 4.2:	Primer Magnitude History for Leg 6 With DSM	40
Figure 4.3:	Primer Magnitude History for Leg 8 in Table 4.1	41
Figure 4.4:	Primer Magnitude History for Leg 8 With DSM	41
Figure 4.5:	Primer Magnitude History for Leg 10 in Table 4.1	42
Figure 4.6:	Primer Magnitude History for Leg 10 With DSM	42
Figure 4.7.1:	Initial Mass vs Launch Date for Round Trip Mars Missions	43
Figure 4.7.2:	Percent Savings of Initial Mass	43

Figure 4.8: Primer Magnitude History for 2020 Abort Mission	44
Figure 4.9: Primer Magnitude History for 2020 Abort Mission With DSM	44
Figure 4.10: Primer Magnitude History for 2022 Abort Mission	45
Figure 4.11: Primer Magnitude History for 2022 Abort Mission With DSM	45
Figure 4.12: 2020 Round Trip Mars Mission	46
Figure 4.13: 2020 Abort Mars Mission Without DSM	46
Figure 4.14: 2020 Abort Mars Mission With DSM	47
Figure 4.15: 2022 Round Trip Mars Mission	47
Figure 4.16: 2022 Abort Mars Mission Without DSM	48
Figure 4.17: 2022 Abort Mars Mission With DSM	48

V. Nomenclature

Abbreviations

ADS	Automated Design Synthesis
BPLANE	pre-existing code for placing deep space maneuvers on interplanetary trajectories
DSM	deep space maneuver
IPOST	Interplanetary Program to Optimize Simulated Trajectories
IPREP	Interplanetary Pre-Processor
MULIMP	Multi-Impulse Software
PRIMER	Software developed to place deep space maneuvers on interplanetary trajectories
SOI	sphere of influence
sol	solar day

Symbols

\bar{a}	control vector
A	matrix as defined in equation 2.21
c	exhaust velocity (m/s)
d	magnitude of $\Delta\vec{V}_{DSM}$
E	specific energy (m^2/s^2)
\bar{f}	state vector time derivative
F	Lagrangian
g_0	acceleration due to gravity at Earth's surface (m/s^2)
\bar{g}_i	components of acceleration vector due to gravity
G_i	see equation A.10

h_k	constraint equations
I	identity matrix
I_{sp}	engine specific impulse (sec)
J	cost function
l_i	direction cosines of thrust vector
l_i^*	all possible values of l_i
m	propellant mass flow rate
m^*	all possible values of m
M	spacecraft mass
p	magnitude of the primer vector
\bar{r}	position vector
\bar{r}_{DSM}	position vector of the deep space maneuver
\bar{r}_{NOM}	position vector on the nominal trajectory
r_p	magnitude of periapsis radius
S	matrix as defined in equation 2.11
t	time (sec)
t_0	initial time
t_f	final time
t_m	time of maximum primer magnitude
tof_n	time of flight on leg number n
u	as defined after equation A.12
U	as defined after equation A.11
\bar{v}	velocity vector
V_∞	hyperbolic excess velocity
$V_{\infty,in}$	inbound hyperbolic excess velocity
$V_{\infty,out}$	outbound hyperbolic excess velocity

V_{peri}	periapsis velocity
W	matrix as defined in equation 2.11
\bar{x}	state vector
\bar{y}	as defined after equation A.5
β	as defined after equation A.5
γ, ν	constants as defined in equation A.12
ΔV	velocity increment (m/sec)
ΔV_n	velocity increment on leg n (m/sec)
ΔV_{DSM}	velocity increment at deep space maneuver
$\partial \bar{r}$	perturbation of position vector
$\partial \bar{v}$	perturbation of velocity vector
ε	perturbation parameter
θ	swingby turn angle (deg)
θ_{max}	maximum swingby turn angle (deg)
κ	switching function
$\bar{\lambda}$	primer vector or (in Appendix) a Lagrange multiplier vector whose first three components form the primer vector
$\dot{\bar{\lambda}}$	first time derivative of the primer vector
μ	gravitational parameter (in equations 2.1 and 2.2) or a Lagrange multiplier vector (in Appendix)
ϕ	state transition matrix
ψ	overall state transition matrix (equation 2.12)
$ (vector) $	magnitude of (vector)

Subscripts

0	initial condition
f	final condition
i	index ranging from 1 to n, or from 1 to 3, as specified
j	index ranging from 1 to m, or from 1 to 3, as specified
k	index ranging from 1 to p
m	number of controls
n	number of states
p	number of constraints
q	number of final states which are fixed
r	dummy index ranging from 1 to n, or from (p+1) to m, as specified
s	index ranging from (q+1) to n
w	index ranging from 1 to q

1. Introduction

Background

With the continuing efforts to develop Space Station Freedom, efforts are also being directed toward the next steps in our space program; a return to the moon, and then a manned expedition to Mars. In relation to these efforts, studies are being performed to determine optimal trajectories for these missions. Trajectories can be simulated and numerically optimized on a computer. These simulations can determine the encounter dates which minimize some cost function, say initial mass of the vehicle or total ΔV . However, other missions with different architectures and lower costs may exist. The addition of a planetary swingby or a deep space maneuver (DSM) changes the architecture of a mission and may reduce the overall cost of the mission.

Since the location of a swingby is determined by the position of the swingby planet, time is the only independent variable for the addition of a swingby. Therefore, to determine if a swingby will reduce the cost of a trajectory, a second simulation can be performed with the swingby architecture. By varying the time of the swingby, the minimum cost of the new architecture can be determined and compared to the cost of the original trajectory. The criteria for determining if a DSM will reduce the cost of a mission is not so simple. One example of when a DSM will be beneficial is in the transfer of a satellite between two non-coplanar orbits. Say there is a satellite at point A in orbit 1 in Figure 1.1, and we want to rendezvous with a second satellite at point B in orbit 2. This rendezvous can always be accomplished with a two burn transfer trajectory. The plane of this trajectory is determined by the points A and B, and the center of attraction of the orbits. As in the figure, this plane may be highly inclined. The out of plane component of the

velocity on the transfer orbit will require large ΔV 's at points A and B. A DSM can be used to reduce these out of plane components, and thus the total ΔV . If the satellite remains in the plane of orbit 1 after the initial burn, an additional burn can be applied when the satellite reaches the line of nodes. This burn would be used only to change the plane of the transfer orbit from that of orbit 1 to that of orbit 2. A final burn can then be applied at Point B to match the velocity of the second satellite. Previous studies¹ have shown that allowing some of the out of plane ΔV 's to take place at Points A and B can reduce the total ΔV required even further. The DSM would not take place right on the line of nodes, but rather some distance from it.

The location and time of a DSM are independent, and therefore the one-dimensional search used for the swingby is no longer applicable. Since a DSM can be located anywhere in space, a four-dimensional search of time and the three coordinates of the DSM requires a great amount of computation. However, if a reliable initial estimate can be generated for the time and location of a DSM, this search can be reduced to a reasonable effort.

Primer vector theory, introduced by Lawden², can be used to make these initial estimates. Previous work on this subject stemming from the work of Lawden has been done by Jezewski and Rozendaal³, Glandorf⁴, and Lion and Handelsman⁵, among others. MULIMP⁶ (Multi-Impulse Trajectory and Mass Optimization Program) is a piece of software which was developed at ITT Research Institute, and later at Science Applications, Inc. for the Jet Propulsion Laboratory in Pasadena, California. MULIMP applies primer vector theory to place DSM's on interplanetary trajectories, and may be the tool most commonly used to do so.

The purpose of this study is to develop new software which uses primer vector theory to locate DSM's quickly on interplanetary trajectories. The software has been integrated into a trajectory analysis code called IPREP (Interplanetary Pre-

Processor)⁷. IPREP previously had the capability to place DSM's on trajectories, however the routine which it used to find DSM's was very slow and not reliable. This paper provides an introduction to primer vector theory, a method to determine the initial estimates for the time and location of a DSM if one will be beneficial, and an algorithm to incorporate DSM's on trajectories with swingby's. Incorporating a DSM on a trajectory with a swingby presents a difficulty because if the DSM precedes the swingby, then the inbound V_{∞} vector to the swingby is not known a priori, and the swingby parameters cannot be calculated. The situation is similar if the DSM follows the swingby or if more than one DSM is used on the same leg of a trajectory.

Thesis Organization

The first major section of this thesis is devoted to reviewing all of the assumptions and approximations used in the analyses which follow. A description of the methods used in IPREP to calculate and optimize trajectories is presented. The derivation and assumptions of primer vector theory will then be summarized. Finally, the process of incorporating primer vector theory into IPREP will be discussed.

Results are discussed in the next section. In order to verify that the new software was functioning properly, a previous study which used DSM's was analyzed with the new software. This study was of a Cycler trajectory between Earth and Mars. A second study was done on round trip Mars missions to show the affect DSM's can have on expanding launch windows. Abort scenarios for Mars missions were also examined to determine how DSM's might be used to open more abort options for manned missions. Finally, conclusions are drawn and recommendations for future work are prescribed.

2. Analysis

Description of IPREP

IPREP was originally intended for use as an aid in using IPOST⁷ (Interplanetary Program to Optimize Simulated Trajectories). IPOST will optimize a trajectory when initial estimates for some of the parameters of that trajectory are input. However, the input parameters must describe a reasonable trajectory to guarantee convergence in IPOST. IPREP determines reliable initial estimates of the V_∞ vectors and encounter dates to be used for inputs into IPOST. However, IPREP can also be used as a stand alone tool for preliminary analysis of interplanetary trajectories.

Inputs to IPREP include the order of the planets to be encountered, maneuvers to be performed at each encounter, and a time of flight window from each encounter to the next. For each of these windows, there is also an input step size which determines how many dates will be checked in that window. For a given set of encounter dates, IPREP calculates the trajectory using a patched-conic technique. In this technique, the planets are assumed to be point masses, and the position and velocity of each planet is found from one of the ephemerides available in IPREP⁸. A transfer orbit for each leg of the trajectory is found by solving Lambert's problem. With these transfer orbits the V_∞ vectors are determined. For launch or orbit insertion maneuvers, a parking orbit must be defined by the user. With the parking orbit defined, the periapsis velocity in the parking orbit is known. The energy equation:

$$E = \frac{|V_\infty|^2}{2} = \frac{|V_{\text{peri}}|^2}{2} - \frac{\mu}{r_p} \quad (2.1)$$

is used to determine $|V_{\text{peri}}|$, the magnitude of the velocity at periapsis along the inbound or outbound hyperbola for orbit insertion or launch, respectively. The difference between this value and the magnitude of the velocity in the parking orbit at periapsis is then the required ΔV , with the assumption being that all ΔV 's are made to be tangential to the orbit at periapsis. Notice that this method produces a magnitude for the ΔV , but the direction of the ΔV vector is not determined.

If the inclination of the parking orbit is defined by the user and is such that a plane change must be performed in order to get from the V_{∞} vector to the parking orbit, this plane change burn is calculated separately and its magnitude (not a vector addition) is added to the ΔV required for the maneuver.

Two methods are available in IPREP to determine the ΔV required for a swingby maneuver. The first and more simple method compares the magnitude of the inbound and outbound V_{∞} vectors and determines the angle between them by taking their scalar product. The angle between the V_{∞} vectors determines the required turn angle, θ , for the swingby, which is also given⁹ by:

$$\sin \frac{\theta}{2} = \frac{1}{1 + \frac{r_p V_{\infty, \text{in}}}{\mu}} \quad (2.2)$$

If the required value of r_p , the swingby radius, falls between the user input values for the minimum and maximum values, then the required swingby ΔV is the difference in magnitude between the inbound and outbound V_{∞} vectors. However, if the required r_p falls outside of the allowed range, the additional turn angle must be made up by the ΔV . In this case, the ΔV becomes:

$$\Delta V = \sqrt{|V_{\infty, \text{in}}|^2 + |V_{\infty, \text{out}}|^2 + |V_{\infty, \text{in}}||V_{\infty, \text{out}}|\cos(\theta - \theta_{\text{max}})} \quad (2.3)$$

This method applies the ΔV after the swingby has been completed, instead of at periapsis.

The second method to calculate swingby ΔV 's uses a non-linear optimizer to find the smallest ΔV which can complete the swingby⁹. The ΔV is applied at periapsis along the inbound hyperbolic trajectory (which in general is not the same as periapsis along the outbound hyperbolic trajectory). The non-linear optimizer is invoked with the radius of periapsis and the direction of the swingby ΔV vector as controls, and the magnitude of the swingby ΔV as a cost function. A lower limit of 1.1 planetary radii is imposed on the periapsis radius to avoid atmospheric interaction.

After all of the ΔV 's have been found, a cost function for that trajectory is evaluated⁴:

$$\text{cost} = \sum_{n=1}^N \left[\frac{|V_{\infty, \text{in}}|_n}{\text{tol}(1, n)} + \frac{|V_{\infty, \text{out}}|_n}{\text{tol}(2, n)} + \frac{\Delta V_n}{\text{tol}(5, n)} + \frac{\Delta V_{\text{DSM}, n}}{\text{tol}(6, n)} + \frac{\text{tof}_n}{\text{tol}(7, n)} \right] + \frac{\text{initial mass}}{\text{tol}(3, 1)} + \frac{\text{final mass}}{\text{tol}(4, N)} \quad (2.4)$$

where N is the number of events in the trajectory, tof_n is the time of flight for the n^{th} leg, and $\text{tol}(1-7, N)$ is a user defined array of weighting parameters. By weighting different parameters in this equation, the user can define the cost function to be the initial mass, total ΔV , or some other function.

IPREP begins by running the trajectory with all of the dates set to the beginning of each encounter window. The last date is incremented and new trajectories are run until the end of the last encounter window is reached. At that point, the second to last date is incremented, the last date is reset to the beginning of its window, and the process continues. The cost function is evaluated for each trajectory, and the set of dates which produces the lowest cost function is saved.

After all of the combinations of dates has been run, the minimum cost trajectory is written to an output file.

This 'grid search' method of optimization has advantages and disadvantages. The disadvantage is that for trajectories with large encounter windows or many events, the number of trajectories to be calculated grows very quickly. For a trajectory with N events and m dates to be checked for each event, the total number of trajectories to be run is m^N . The advantage to the grid search method is that it will not become trapped in a local minimum as gradient methods do. IPREP does also allow the user to define a maximum total trip time, which may eliminate some of the combinations of dates before those trajectories are run.

Primer Vector Theory

The derivation of four necessary conditions for optimality on impulsive trajectories where the total ΔV is minimized was presented by Lawden². That derivation is summarized in the Appendix of this report. The conditions derived are:

- 1) The primer vector and its first time derivative are continuous.
- 2) During any impulse, the thrust vector must be aligned with the primer.
- 3) The magnitude of the primer is a maximum and has a value of one during any impulse.
- 4) The derivative of the magnitude of the primer is zero at a deep space maneuver.

In arriving at these conditions, the spacecraft was treated as a point mass in an inverse square law gravitational field. The thrusts were modeled as impulses, and assumed to occur over infinitesimal time duration. Also, the cost function was taken to be the total ΔV , which is given by the rocket equation as:

$$\Delta V = g_0 I_{sp} \left(\ln \left| \frac{M_i}{M_f} \right| \right) \quad (2.5)$$

It should be noted that the cost function here is different than the cost function used in the grid search optimization in IPREP. However, minimizing total ΔV is equivalent to minimizing the initial mass of the vehicle if no discontinuities in the mass of the vehicle are incurred. Mass discontinuities occur if part of the vehicle (say a Mars excursion vehicle) is jettisoned. In general, this only occurs at the end of a leg of the trajectory, and since primer vector theory will be applied to each leg of the trajectory separately, total ΔV is a good choice for the cost function here.

It is noted from equations A.20 and A.21 in the appendix of this report, that the primer vector, $\bar{\lambda}$, satisfies the same differential equation as the 'deviation vector' in equation 9.31 of Reference 10. The solution to this equation is given by equation 9.45 in Reference 10 as:

$$\left[\frac{\partial \bar{r}}{\partial \bar{v}} \right]_t = \psi(t, t_0) \left[\frac{\partial \bar{r}}{\partial \bar{v}} \right]_{t_0} \quad (2.6)$$

Therefore, the primer vector can be found at any point along a trajectory from the equation:

$$\begin{bmatrix} \bar{\lambda} \\ \dot{\bar{\lambda}} \end{bmatrix}_t = \psi(t, t_0) \begin{bmatrix} \bar{\lambda}_0 \\ \dot{\bar{\lambda}}_0 \end{bmatrix} \quad (2.7)$$

where $\psi(t, t_0)$ is the overall state transition matrix. If ψ and the initial conditions on the primer vector and its derivative are known, then the primer and its derivative can be found along the entire trajectory. Assuming we have a mission which begins with a launch and ends with an orbit insertion, then the primer vector at the initial and final times is known to be a unit vector in the direction of the thrust at those points. The parameters of the parking orbits at each end of the trajectory provide the information to determine the position and velocity of the

spacecraft at periapsis. From this information, and from a Lambert solution between the initial and final position of the spacecraft, the direction and magnitude of the initial and final ΔV 's can be determined. Equation 2.7 becomes:

$$\begin{bmatrix} \bar{\lambda} \\ \dot{\bar{\lambda}} \end{bmatrix}_{t=t_f} = \psi(t_f, t_0) \begin{bmatrix} \bar{\lambda}_0 \\ \dot{\bar{\lambda}}_0 \end{bmatrix} = \begin{bmatrix} \psi_{11} & \psi_{12} \\ \psi_{21} & \psi_{22} \end{bmatrix} \begin{bmatrix} \bar{\lambda}_0 \\ \dot{\bar{\lambda}}_0 \end{bmatrix} \quad (2.8)$$

where the 6X6 matrix $\psi(t_f, t_0)$ has been replaced with the equivalent four 3X3 matrices. These leads to⁵:

$$\bar{\lambda}_f = \psi_{11}\bar{\lambda}_0 + \psi_{12}\dot{\bar{\lambda}}_0 \quad (2.9)$$

$$\dot{\bar{\lambda}}_0 = \psi_{12}^{-1}[\bar{\lambda}_f - \psi_{11}\bar{\lambda}_0] \quad (2.10)$$

If ψ_{12} is not singular, we can find the initial conditions on the derivative of the primer vector. With these conditions known, the primer vector can be propagated along the entire trajectory.

A problem occurs when we cross into or out of a sphere of influence (SOI). The sphere of influence is an imaginary boundary, where inside the sphere all motion is assumed to be governed solely by the gravitational attraction of the planet, and outside of the sphere, motion is assumed to be governed by the gravitational attraction of the sun. To further develop the idea of the SOI, consider a spacecraft in space near a planet. Its motion can be modeled as a two body problem, where the spacecraft and the planet are orbiting around their common center of gravity. The attraction of the sun, which is considerably farther away, can be approximated as a disturbing force in that two body problem. As the spacecraft moves away from the planet, the ratio of the disturbing force from the sun to the force from the planet increases. As we move farther from the planet, the motion

can be modeled as the spacecraft orbiting the sun, and the attraction of the planet could then be considered the disturbing force. At some distance from the planet, the ratio of the disturbing force to the central force will be the same for each of these two models. The mean distance at which this is true is defined as the radius of the sphere of influence for the planet. The magnitude of this radius will be dependent on the direction the spacecraft has moved from the planet. However, if the distance between the sun and the planet is much greater than this radius, then the radius is approximately constant for all directions¹⁰, and the SOI is approximated to be a true sphere. The value for the radius of the SOI for each planet is provided by the ephemeris information in IPREP⁸.

Since the initial and final conditions on the primer are determined by the ΔV vectors inside the SOI, the primer vector must first be propagated from its initial condition out to the boundary of the SOI. When the primer exits the SOI, Glandorf has shown⁴ that the primer is continuous, but its derivative is not. Fortunately, the discontinuity in the derivative is not arbitrary, and can be calculated. To generate the primer across a sphere of influence:

$$\begin{bmatrix} \bar{\lambda} \\ \dot{\bar{\lambda}} \end{bmatrix}_+ = W \begin{bmatrix} \bar{\lambda} \\ \dot{\bar{\lambda}} \end{bmatrix}_- = \begin{bmatrix} I & 0 \\ S & I \end{bmatrix} \begin{bmatrix} \bar{\lambda} \\ \dot{\bar{\lambda}} \end{bmatrix}_- \quad (2.11)$$

The + indicates a value immediately after crossing the boundary, and the - indicates the value immediately before crossing the boundary. S is a 3X3 matrix⁴, dependent on the position and velocity of the sphere of influence with respect to the sun, and the velocity of the spacecraft with respect to the sphere. The S matrix is also dependent on whether the spacecraft is entering or leaving the sphere. With this in mind, the overall state transition matrix can be formed:

$$\psi(t_f, t_0) = \phi(t_f, t_2)W(t_2)\phi(t_2, t_1)W(t_1)\phi(t_1, t_0) \quad (2.12)$$

where t_1 is the time when the spacecraft leaves the first SOI and t_2 is the time when the spacecraft enters the second SOI. $\phi(t_f, t_2)$ and $\phi(t_1, t_0)$ are the state transition matrices for the travel in the second and the first SOI's, respectively, and $\phi(t_2, t_1)$ is the state transition matrix for travel between these two SOI's. If the trajectory consists of a launch, followed by an unpowered swingby and then an orbit insertion, the overall state transition matrix must be adjusted. This means a total of four extra matrices need to be multiplied into $\psi(t_f, t_0)$; one state transition matrix to get from the previous SOI to the swingby SOI, one W matrix to get in the SOI, another state transition matrix to get through the SOI, and one more W matrix to get out of the SOI.

With the overall state transition matrix and the initial conditions on the primer and its derivative known, the primer can be generated by equation 2.7. When this is complete, the primer history can be analyzed to find if there are indications that a DSM would be beneficial. By propagating the primer with the state transition matrices, the primer is guaranteed to be continuous. Its derivative will also be continuous everywhere except at the boundaries of the SOI's. This discontinuity is only a result of the mathematics involved in changing coordinate systems and the center of attraction governing the motion, and is not an indication of a non-optimum trajectory. The primer has been defined as a unit vector along the ΔV vectors, so the first and second necessary conditions stated earlier are satisfied. Since a DSM has not yet been added, the fourth condition is also not satisfied. Only the third condition is left to be satisfied. If the maximum magnitude of the primer along its history is greater than one, the trajectory is not optimal, and a DSM will be beneficial. To first order, the best time for the DSM is at the time when the primer magnitude is greatest³. Some representative optimal and non-optimal primer magnitude histories are shown in Figures 1.2 - 1.5.

Approximating the Location of a DSM³

The state transition matrix $\phi(t_1, t_0)$ defines how the state of a spacecraft at time t_1 will be affected by changes in the state at time t_0 :

$$\phi(t_1, t_0) = \begin{bmatrix} \frac{\partial \bar{r}(t_1)}{\partial \bar{r}_0} & \frac{\partial \bar{r}(t_1)}{\partial \bar{v}_0} \\ \frac{\partial \bar{v}(t_1)}{\partial \bar{r}_0} & \frac{\partial \bar{v}(t_1)}{\partial \bar{v}_0} \end{bmatrix} = \begin{bmatrix} \phi_{11} & \phi_{12} \\ \phi_{21} & \phi_{22} \end{bmatrix} \quad (2.13)$$

To find the location of a DSM, consider perturbations about the trajectory to which a DSM is being added. The nominal and perturbed trajectories are shown in figure 2.1. Take the point on this nominal trajectory where the primer has its maximum magnitude (call this time t_m), and perturb the location by some amount, $\partial \bar{r}(t_m)$. From the definition of the state transition matrix:

$$\begin{bmatrix} \partial \bar{r}(t_m) \\ \partial \bar{v}(t_m) \end{bmatrix}_- = \phi(t_m, t_0) \begin{bmatrix} \partial \bar{r}_0 \\ \partial \bar{v}_0 \end{bmatrix} \quad (2.14)$$

$$\begin{bmatrix} \partial \bar{r}(t_m) \\ \partial \bar{v}(t_m) \end{bmatrix}_+ = \phi(t_m, t_f) \begin{bmatrix} \partial \bar{r}(t_f) \\ \partial \bar{v}(t_f) \end{bmatrix} \quad (2.15)$$

The endpoints on the trajectory are fixed, and so $\partial \bar{r}(t_f) = \partial \bar{r}(t_0) = 0$. Also note that $\partial \bar{r}(t_m)_- = \partial \bar{r}(t_m)_+$ for continuity.

From equations 2.14 and 2.15:

$$\partial \bar{v}(t_m)_+ - \partial \bar{v}(t_m)_- = \phi_{22}(t_m, t_f) \partial \bar{v}(t_f) - \phi_{22}(t_m, t_0) \partial \bar{v}(t_0) \quad (2.16)$$

$$\partial \bar{v}(t_f) = \phi_{12}^{-1}(t_m, t_f) \partial \bar{r}(t_m)_+ \quad (2.17)$$

$$\partial \bar{v}(t_0) = \phi_{12}^{-1}(t_m, t_0) \partial \bar{r}(t_m)_- \quad (2.18)$$

$$\partial\bar{v}(t_m)_+ - \partial\bar{v}(t_m)_- = [\phi_{22}(t_m, t_f)\phi_{12}^{-1}(t_m, t_f) - \phi_{22}(t_m, t_0)\phi_{12}^{-1}(t_m, t_0)]\partial\bar{r}(t_m) \quad (2.19)$$

or

$$\partial\bar{r}(t_m) = A^{-1}[\partial\bar{v}(t_m)_+ - \partial\bar{v}(t_m)_-] \quad (2.20)$$

where

$$A = [\phi_{22}(t_m, t_f)\phi_{12}^{-1}(t_m, t_f) - \phi_{22}(t_m, t_0)\phi_{12}^{-1}(t_m, t_0)] \quad (2.21)$$

The thrust vector of the DSM must be aligned with the primer vector on the new trajectory. For small perturbations, the direction of the primer on the new trajectory can be taken to be the same as for the nominal trajectory. This yields the equation:

$$\partial\bar{r}(t_m) = dA^{-1} \frac{\bar{\lambda}(t_m)}{|\bar{\lambda}(t_m)|} \quad (2.22)$$

where d is the magnitude of the DSM ΔV . Jezewski and Rozendaal³ expressed the total ΔV on the trajectory as a second order function of d . Taking the derivative of this expression with respect to d , and setting the resulting expression equal to 0, they arrived at an expression for d to be used in finding $\partial\bar{r}(t_m)$. The expression can be added to the radius on the nominal trajectory to arrive at the position of the DSM:

$$\bar{r}_{\text{DSM}} = \bar{r}_{\text{NOM}}(t_m) + \partial\bar{r}(t_m) \quad (2.23)$$

A non-linear optimizer is then invoked with the initial estimates for the three coordinates of the DSM and t_m as four independent variables, and total ΔV as a cost function. The original trajectory now consists of two legs: one from t_0 to t_m , and the second from t_m to t_f . The primer vector can then be found along each of these new legs, and the optimality conditions can be checked again.

Finding DSM's on Trajectories with Swingby's

The problem previously mentioned in incorporating a DSM either before or after a swingby has been solved by using the method of the previous section. With an initial estimate for the location and time of the DSM, the swingby parameters can be calculated, and the total ΔV for the trajectory can then be found. Two options are available to calculate the primer along a trajectory which uses a powered swingby. The first is to treat both the powered and unpowered swingby scenarios similarly. This would involve propagating the primer vector all the way through the SOI of the swingby planet. For a powered swingby where the impulse takes place at periapsis of the inbound hyperbolic trajectory, one state transition matrix for the inbound hyperbolic orbit, and a second state transition matrix for the outbound hyperbolic orbit are needed. As mentioned previously, an unpowered swingby involves four additional matrix multiplications in the calculation of $\psi(t_f, t_0)$. A powered swingby would therefore require five multiplications. This method guarantees continuity of the primer and its derivative at the swingby, but it does not guarantee that the primer will be a unit vector aligned with the thrust at the point when the impulse for the swingby is applied.

The second option is to analyze the trajectory in two separate parts. The first part is from the beginning of the leg to the swingby, and the second is from the swingby to the end of the leg. This method can only be used on powered swingby's, since an unpowered swingby does not provide a thrust vector which determines the boundary conditions on the primer vector. This method guarantees that the primer will be a unit vector aligned with the thrust at the swingby (since it will be defined as such), but it does not guarantee continuity of the derivative of the primer at the swingby. After a comparison of these two methods, which will be discussed later, the second option was selected.

3. Software Developed

Integration into IPREP

The methods described earlier to find the time and location of a DSM along an interplanetary trajectory were implemented in a computer program. The program is written in FORTRAN, and was originally written to run independently of any other software. It has recently been integrated into IPREP. Presently, it takes a trajectory from IPREP, finds the overall state transition matrix for each leg of the trajectory, and computes the primer vector along the entire trajectory. Then, the primer vector history is examined to find if and when the magnitude exceeded unity. If it has, a routine is called to generate the initial estimate for the location of a DSM, and this estimate along with the time of the DSM are sent to an optimizer, where total ΔV is the objective function. When the optimization is complete, the new trajectory is compared to the original to verify that the cost function has been reduced by the DSM.

A considerable amount of work had to be performed in order to calculate the overall state transition matrix with the information in IPREP. As noted previously, with the technique used in IPREP, the magnitudes of the required ΔV 's are found, but the direction of the burns is never calculated. This information is necessary to provide the boundary conditions on the primer vector, and therefore must be extracted.

For a launch, the direction of the ΔV is the same as the direction of the velocity vector at periapsis, while for an orbit insertion, the direction of the ΔV is the opposite as the direction of the velocity vector at periapsis. In order to determine the direction of the ΔV , the part of the trajectory which takes place within the SOI must be taken into account. The turn angle which is incurred by the

velocity vector while within the SOI is one half of the turn angle of a swingby with the same V_∞ vector and periapsis radius, and can therefore be found with equation 2.2. So the direction of the periapsis velocity can be found by rotating the V_∞ vector in the plane of the hyperbolic orbit by this turn angle. The plane of the hyperbolic orbit must be defined. The inclination of the orbit is taken to be equal to the declination of the V_∞ vector. As before, any plane change necessary to comply with input restrictions on the parking orbit will be treated as a separate burn. Then, the line of nodes is taken to be perpendicular to the V_∞ vector. The line of nodes and the inclination completely define the plane of the orbit, and there is now enough information to determine the direction of the burn. The direction of a swingby ΔV can be found in a similar manner for both the optimized and the simple swingby methods.

Optimizer

Two optimizers were implemented in the software to determine which optimizer was the better in terms of speed and finding a lower total ΔV . The first was a simple, first order optimizer which was written explicitly for this application. There are four independent variables; the three coordinates for the location of the DSM, and the time of the DSM. The initial estimates for these variables, which can be obtained as described earlier, are input to the optimizer. The original two burn trajectory is now broken into two separate trajectories. The Lambert problem is solved from the location of the first burn to the location of the DSM, and a second Lambert problem is solved from the location of the DSM to the location of the second burn. With the required transfer trajectories now known, the three ΔV 's can be found, and the sum of them is saved. The optimizer then increments each of the three coordinates of the location of the DSM by a pre-defined step size. For the first

increments, this step size is taken to be one tenth of the magnitude of the position vector on the original two burn trajectory at the time of the DSM. The X, Y, and Z components of the location are incremented in both the positive and negative directions, and for each case, the sum of the ΔV 's is found. The new location of the DSM is then assigned to be whichever of these six steps produced the greatest decrease in the sum of the ΔV 's. If none of the six steps produced a reduction in ΔV , then the step size is halved for the next iteration.

After the six steps for the location of the DSM have been tried, and the one with the best result is taken, the time of the DSM is incremented. The initial step size for the time increment is one tenth of the time of flight of the original trajectory. As with the other variables, the time step is applied both in the positive and negative directions, and the one which results in the greater decrease in ΔV is assigned as the new time for the DSM. If neither results in a decrease in ΔV , then the time step is halved, and the optimization continues with the location variables.

Upper and lower bounds are applied on the time variable, so that the time step will not place the DSM outside of the time of flight for the original trajectory. No boundaries are put on the location variables. If one of the steps puts the location of the DSM in an unfavorable location, the ΔV will increase, and the optimizer will not take that step. The optimization is considered complete when the location step size is 0.01 of its original size, and the time step is less than 0.1 days.

The second optimizer which was considered was a commercially available code known as ADS (Automated Design Synthesis)¹¹. ADS offers a variety of optimization techniques including a conjugate gradient method and a variable metric technique. ADS allows the user to either supply gradient information, or ADS can calculate gradients internally. For this application, all the gradients were calculated internally by ADS, which uses a finite difference method. It was hoped

that ADS would converge on a minimum faster than the other, less sophisticated optimizer, but this was not found to be the case. The amount of time ADS required to complete the optimization was dependent on the method of optimization used in ADS. Most of the methods took significantly longer than the first optimizer. The method in ADS which converged as fast as the other optimizer found a solution which did not have as low a ΔV as the first optimizer. For this reason, the first optimizer is the one that was selected for the software.

4. Results

Cycler Trajectory Analysis

Once the software had been written, a verification that it was working properly was desired. This verification was done by use of a study which had been done previously¹². This study incorporated DSM's on an interplanetary cycler trajectory with the use of the DSM routine currently in IPREP. The cycler in this study is a spacecraft which is put into an orbit which continually cycles past both Earth and Mars. At each encounter, a swingby is performed to send the cycler back to the other planet. The cycler which was analyzed had eight Earth swingby's and seven Mars swingby's between the years 1996 and 2011.

The results from this previous study were reproduced using the DSM routine (BPLANE) which is currently in IPREP. The same mission was then analyzed with the new DSM routine (PRIMER). When this trajectory was analyzed using the first option described earlier for trajectories with swingby's, a problem occurred. The additional matrix multiplications involved in each of the swingby's led to round off error in the overall state transition matrix. The propagation of the primer vector is very sensitive to the initial conditions, and the error in the overall state transition matrix caused the primer to fail to meet the final boundary conditions. For this reason, the second option (splitting the trajectory at each swingby) was seen to be the better.

Table 4.1 shows the ΔV requirements for the nominal mission (where no DSM's are used). The ΔV 's on legs 6 through 10 are significantly greater than those on the other legs, and so the analysis performed in Reference 11 involved looking for DSM's only on legs 6, 8, and 10. The last two columns in Table 4.1 show the ΔV requirements for the trajectories which were found with the BPLANE routine and

the PRIMER routine. Each was able to locate DSM's which significantly reduce the ΔV requirements of the mission. The fact that the new PRIMER routine found a trajectory with a slightly lower total ΔV is not as significant as that it did so in approximately one third the time.

A closer look at leg 6 proves revealing. The DSM which was found by the BPLANE routine reduces the sum of the ΔV 's for the two swingby's surrounding that leg to 0.562 km/sec. The total ΔV for the same leg on the PRIMER trajectory is 0.624 km/sec. On this particular leg, the BPLANE routine found a more efficient DSM. Figure 4.1 reveals that the initial estimate for the time of the DSM made by the PRIMER routine was July 29, 2002. Figure 4.2 then shows that the optimizer moved this date back to July 23, 2002. However, the optimizer was unable to find the more efficient DSM on May 25, 2002 which was found by the BPLANE routine. The conclusion can be drawn that each routine is susceptible to local minima in the optimization process. Figures 4.3 to 4.6 show the primer magnitude histories for legs 8 and 10.

A second analysis was performed on the same mission. Using the same encounter dates for each of the swingby's as the previous analysis, DSM's were sought on each leg. The results for this study are in Table 4.2. Surprisingly, the BPLANE routine finds a mission with a higher total ΔV than the BPLANE routine with three DSM's. Most of this increase in ΔV occurs at the Mars swingby before leg 2. The reason that the BPLANE routine places a DSM on this leg is that the optimization in the BPLANE routine cannot account for the ΔV of a swingby which follows a DSM. The BPLANE routine is invoked in IPREP as soon as there is a leg which calls for a DSM. If this leg ends with a swingby, the ΔV cannot be found since the next leg has not yet been found to determine the outbound V_∞ vector for the swingby. This problem does not occur if the leg ends with an orbit insertion. The

PRIMER routine lets IPREP calculate the entire trajectory before it is invoked. Then, with all of the ΔV 's known, the primer analysis can be done, and the DSM's are inserted last. The PRIMER routine is able to find a total of 7 DSM's on the cycler trajectory and reduces the total ΔV to 2.212 km/sec.

Launch Window Analysis

Another analysis involved the determination of the initial mass of a spacecraft which was to perform a direct (no swingby's), round trip mission to Mars. The initial mass which was needed to perform the mission was plotted against the launch date of the mission in Figure 4.7.1. Launches were taken every 5 days over a period of 500 days, starting from January 1, 2010. Outbound and inbound flight times were varied for each launch date in order to find the combination of encounter dates which produce a minimum initial mass. The Mars stay time was fixed at 60 days for all trajectories. The parameters of the mission are summarized in Table 4.3 and were the same for cases with or without DSM's. Parking orbit inclinations were not specified, and so IPREP always selects the inclination to equal the declination of the inbound or outbound V_∞ vector for orbit insertion or launch, respectively.

Figure 4.7.1 shows noticeable improvements by using DSM's over the second half of the time period examined. Smaller improvements were also made for launch dates in January and February of 2010. Of the 101 launch dates examined, 98 were improved by the use of DSM's. Figure 4.7.2 shows the percentage of mass on the nominal mission which is saved by the use of DSM's. The discontinuity on this plot is caused by the three dates where no DSM could be found, since the zero percent savings cannot be plotted on the logarithmic scale. The purpose of this study was not to do a detailed examination of when launch opportunities occur, but rather to show that DSM's can expand the launch windows. Figure 4.7.1 shows that

by using DSM's, the minimum initial mass pertaining to a specific launch date may be reduced below a specified maximum allowable initial mass, thus including that date in a launch window.

Abort Mission Analysis

Two round trip Mars missions were selected to serve as nominal cases for an abort mission analysis. These missions were selected because they have a relatively low total ΔV and initial mass, and could be considered practical candidates for a manned Mars mission. Again, this study was done to show the usefulness of the DSM capability in IPREP, and not as an in-depth mission analysis.

The launch date of the first mission is in the year 2020, and the mission parameters are outlined in Table 4.4. The nominal mission (where there is no abort) has a two year trip time, including 60 days stay time at Mars. The abort mission assumes that some problem occurred after launch, and the spacecraft is to return to Earth at least 50 days earlier than the nominal mission. To accomplish this, the orbit insert at Mars is replaced with a swingby. The Mars encounter date for the abort mission is the same as for the nominal mission, while the Earth return date is allowed to vary up to the maximum trip time to find the minimum initial mass needed to complete the mission. The abort mission was run with and without searching for a DSM on the return leg. A DSM was not used on the first leg, since it is assumed that the problem occurred after launch, and the vehicle has achieved the desired trajectory which will rendezvous with Mars. The second mission has a launch date in the year 2022. Its parameters are also outlined in Table 4.4, and the abort scenario is the same as for the first case.

The desired result is for the abort trajectory to require less initial mass than the nominal case. When this is true, the abort trajectory is available at no additional

cost. If the abort trajectory requires a slightly greater initial mass, then it may still be practical to include this extra propellant mass on the nominal mission in order to have the abort trajectory available should a problem occur. The results of this study are shown in Tables 4.5.1 and 4.5.2. Unfortunately, a practical abort trajectory was not available on either of these two missions. However, DSM's were able to improve the abort trajectories in each case. Although the improvement was not great enough to make these abort trajectories feasible, the indication is that for future abort mission analyses, it is worthwhile to search for DSM's. Other abort studies have tried using Venus swingby's to open up abort trajectories. Having the DSM capability in IPREP creates more possibilities for abort analysis such as using Venus swingby's in combination with DSM's.

Figures 4.8 and 4.9 show the primer magnitude history for the 2020 abort mission with and without the DSM, respectively. Figures 4.10 and 4.11 are similar figures for the 2022 abort missions. The trajectories for the nominal and abort missions for both the 2020 and the 2022 missions are shown in figures 4.12 to 4.17.

5. Conclusions

Primer vector theory is useful in determining if a trajectory will be improved by the use of a DSM. Once the primer magnitude history has determined that a DSM should be incorporated, primer vector theory also provides a method to determine initial estimates for when and where to place the DSM. The problem of being unable to calculate swingby parameters when a swingby is either preceded or followed by a DSM is avoided by the use of primer vector theory. This allows any trajectory to be subject to a primer analysis.

The software developed was shown to work effectively and efficiently in improving interplanetary trajectories with deep space maneuvers.

The cycler trajectory analysis verified that the software developed will find DSM's which reduce the ΔV required on a trajectory. The results compared favorably to the BPLANE routine in IPREP which also finds DSM's. The greatest advantage of the new software is the reduction in time required to find DSM's. Although each routine found trajectories with comparable ΔV 's, the dates of the DSM's vary considerably, indicating that each code is susceptible to local minima in the optimization of the DSM's. However, the new software is more robust, in that it will never increase the total ΔV on a trajectory, while the BPLANE code may do so.

The launch window analysis showed another use for DSM's. DSM's were shown reduce a vehicle's initial mass required to complete a mission. If a maximum initial mass is defined, it is apparent that DSM's may be able to reduce the initial mass associated with some launch dates from above this maximum to below it, thus expanding the launch windows for that mission.

The final study showed that DSM's are also useful in looking for possible abort trajectories. Although no practical abort trajectories were found for the two

mission examined, the data indicated that some abort trajectories will become available with the use of DSM's.

6. Recommendations for Future Work

The software developed can be used to perform more detailed analyses of the type which were done for this paper. Launch window analyses for direct Mars missions as well as missions which use Venus swingby's on the inbound or outbound leg can be performed. More in-depth abort analyses can be performed. 'Grand Tour' missions which pass by many planets on the way out of the solar system can be done with DSM's on some or all of the legs.

As for more development in the software, the most important suggestion would be to have the capability to look for more than one DSM on one leg of a trajectory. The software to propagate the primer vector along a trajectory after a DSM has been inserted has already been written. With the primer magnitude history known, all that remains to be done is to generate an initial estimate for the location of the second DSM, and then to invoke an optimizer. The optimizer would have to be altered for the second DSM. The time and three position coordinates of both the first and second DSM's could be used as independent variables in the optimization, and the optimizer currently in use was written specifically for the optimization of one DSM with four independent variables. Figures 4.2, 4.4, and 4.6 indicate that a second DSM could be used on those legs to further reduce the ΔV .

Non-linear methods could be applied to the problem when primer vector theory fails due to the limits imposed by the linear approximations. Non-linear methods could improve the initial estimate for the location of the DSM when that location is distant from the nominal trajectory, and make the software more robust.

7. References

1. Fimple, W.R., "Optimal Midcourse Plane Change for Ballistic Interplanetary Trajectories, AIAA Journal, Vol. 1, No. 2, Jan. 1963, pp. 430-434.
2. Lawden, D.F., *Optimal Trajectories for Space Navigation*, Butterworths, London, 1963, pp. 3-25, 54-66.
3. Jezewski, D.J., and Rozendaal, H.L., "An Efficient Method for Calculating Optimal Free-Space N-Impulse Trajectories," AIAA Journal, Vol. 6, No. 11, Nov. 1968, pp. 2160-2165.
4. Glandorf, David R., "Primer Vector Theory for Matched-Conic Trajectories," AIAA Journal, Vol. 8, No. 1, January 1970, pp. 155-156.
5. Lion, P.M., and Handelsman, M., "Primer Vector on Fixed-Time Impulsive Trajectories, AIAA Journal, Vol. 6, No. 1, Jan. 1968, pp. 127-132
6. Friedlander, Alan L., "MULIMP - Multi-Impulse Trajectory and Mass Optimization Program", Report No. SAI 1-120-383-T4, Science Applications, Inc., for Jet Propulsion Laboratory, April 18, 1975.
7. Hong, P.E., Kent, P.D., Olson, D.W., and Vallado, C.A., "Interplanetary Program to Optimize Simulated Trajectories (IPOST) User's Guide", Martin Marietta Astronautics, Space Launch Systems Company, Denver, Colorado, NASA 1-18230, Volume I, October, 1992.
8. Hong, P.E., Kent, P.D., Olson, D.W., and Vallado, C.A., "Interplanetary Program to Optimize Simulated Trajectories (IPOST) Analytical Manual", Martin Marietta Astronautics, Space Launch Systems Company, Denver, Colorado, NASA 1-18230, Volume II, October, 1992.
9. Striepe, Scott Allen, "Effect of Interplanetary Trajectory Options on Entry Velocities at the Earth and Mars Atmospheric Interface," Thesis, May 1991, The University of Texas at Austin.
10. Battin, Richard H., *An Introduction to the Mathematics and Methods of Astrodynamics*, Second Printing, AIAA, Inc. New York, NY, 1987, pp. 450-463.
11. Vanderplaats, G.N., "ADS - A Fortran Program for Automated Design Synthesis - Version 1.10", NASA Contractor Report 177985, Sep. 1985.
12. Fruth, Gregory, "Establishing an Aldrin Cyler Between Earth and Mars Using Nuclear Electric Propulsion," Thesis, February, 1993, The George Washington University, Washington, D.C.

13. Baker, Jerome M., "Orbit Transfer and Rendezvous Maneuvers between Inclined Circular Orbits", *Journal of Guidance, Control and Dynamics*, Vol. 3, No. 8, Aug. 1966, pp. 1216-1220.
14. Bate, Roger, Mueller, Donald, and White, Jerry, *Fundamentals of Astrodynamics*, Dover Publications, 1971.
15. Bryson, A.E. Jr., Denham, W.F., and Dreyfus, S.E., "Optimal Programming Problems with Inequality Constraints, I: Necessary Conditions for Extremal Solutions", *AIAA Journal*, Nov. 1963.
16. Bryson, Arthur E., and Ho, Yu-Chi, *Applied Optimal Control*, Hemisphere Publishing Corp., New York, NY, 1975.
17. Eckel, Karl, "Numerical Solutions of Non-Coaxial Optimum Transfer Problems, The Journal of the Astronautical Sciences, Vol. X, No. 3, pp. 82-92, Fall 1963.
18. Eckel, Karl, "Optimum Transfer Between Non-Coplanar Elliptical Orbits", Oct. 1961.
19. Eckel, Karl, "Optimum Transfer in a Central Force Field with n Impulses", Aug. 20, 1963.
20. Edelbaum, T.N. "How Many Impulses?", *AIAA Paper No. 66-7*, AIAA 3rd Aerospace Sciences Meeting, New York, Jan. 24-26, 1966.
21. Edelbaum, T.N., "Minimum Impulse Transfers in the Near Vicinity of a Circular Orbit", *The Journal of Astronautical Sciences*, Vol. XIV, No. 2, pp. 66-73, Mar.-Apr. 1967.
22. Gerald, Curtis F., and Wheatley, Patrick O., *Applied Numerical Analysis*, Fourth Edition, Addison-Wesley Publishing Company, New York, 1989.
23. Glandorf, David R. "Lagrange Multipliers and the State Transition Matrix for Coasting Arcs" *AIAA Journal, Technical Notes*, Volume 7, Number 2, Feb. 1969, pp. 363-365.
24. Hiller, H. "Optimum Impulsive Transfers Between Elliptic and Non-Coplanar Circular Orbits", *Planet, Space, Science*, Vol. 13, pp. 1233-1247, Programming Press, Ltd., 1965.
25. Hiller, H. "Optimum Impulsive Transfers Between Non-Coplanar Elliptic Orbits Having Colinear Major Axes", *Planet, Space, Science*, Vol. 14, pp. 773-789, Programming Press, Ltd., 1965.

26. Hiller, H. "Optimum Transfers Between Non-Coplanar Circular Orbits", *Planet, Space, Science*, Vol. 13, pp. 147-161, Programming Press, Ltd., 1965.
27. Jezewski, Donald J., "Primer Vector Theory and Applications", NASA TR R-454, Nov. 1975.
28. Kirk, Donald E., *Optimal Control Theory, An Introduction*, Prentice Hall, New Jersey, 1970.
29. Marec, J.P. *Optimal Space Trajectories*, Elsevier Scientific Publishing Company, New York, 1979.
30. Meirovitch, Leonard, *Methods of Analytical Dynamics*, McGraw-Hill, 1970.
31. Miele, A., Wang, T., and Basupar, V.K., "Primal and Dual Formulations of Sequential Gradient-Restoration Algorithms for Trajectory Optimization Problems", *Acta Astronautica*, Vol. 13, No. 8, pp. 491-505, 1986.
32. Prussing, John E., and Chiu, Jeng-Hua, "Optimal Multi-Impulse Time-Fixed Rendezvous Between Circular Orbits", *Journal of Guidance, Control and Dynamics*, Vol. 9, No. 1, Jan.-Feb. 1986, pp. 17-22.

8. Tables

Table 4.1: Comparison of BPLANE Code and PRIMER Code for Cycler Trajectory from Reference 12

LEG NUMBER	SWINGBY PLANET	DATE	NOMINAL	BPLANE	PRIMER
			ΔV (KM/SEC)	ΔV (KM/SEC)	ΔV (KM/SEC)
1	EARTH	19 NOV 1996	0.073	0.073	0.073
2	MARS	1 MAY 1997	0.081	0.081	0.081
3	EARTH	1 JAN 1999	0.067	0.067	0.067
4	MARS	28 MAY 1999	0.064	0.064	0.064
5	EARTH	8 FEB 2001	0.098	0.098	0.098
6	MARS	6 JUL 2001	1.536	0.000	0.004
	DSM	25 MAY 2002		0.462	
		23 JUL 2002			0.488
7	EARTH	16 APR 2003	2.467	0.100	0.132
8	MARS	12 SEP 2003	2.247	0.000	0.001
	DSM	9 AUG 2004		0.582	
		15 JUL 2004			0.619
9	EARTH	7 JUL 2005	3.699	0.116	0.042
10	MARS	13 DEC 2005	1.062	0.000	0.002
	DSM	17 OCT 2006		0.381	
		27 JUL 2006			0.419
11	EARTH	6 SEP 2007	0.261	0.126	0.023
12	MARS	16 FEB 2008	0.105	0.105	0.105
13	EARTH	10 OCT 2009	0.074	0.074	0.074
14	MARS	28 MAR 2010	0.125	0.125	0.125
	EARTH	13 NOV 2011	0.110	0.110	0.110

TOTAL ΔV (KM/SEC)	12.069	2.565	2.528
RUN TIME (SEC)	3.7	53.2	19.1

Table 4.2: Comparison Between BPLANE Code and PRIMER Code for Cycler Trajectory When a DSM is Allowed on Each Leg

LEG NUMBER	SWINGBY PLANET	DATE	BPLANE	PRIMER
			ΔV (KM/SEC)	ΔV (KM/SEC)
1	EARTH	19 NOV 1996	0.000	0.073
	DSM	20 DEC 1996	0.072	
2	MARS	1 MAY 1997	1.501	0.003
	DSM	27 MAY 1998		0.041
3	EARTH	1 JAN 1999	0.645	0.027
	DSM			
4	MARS	28 MAY 1999	0.000	0.002
	DSM	26 JUL 2000	0.030	
		23 MAY 2000		0.060
5	EARTH	8 FEB 2001	0.000	0.070
	DSM	8 MAR 2001	0.103	
6	MARS	6 JUL 2001	0.000	0.004
	DSM	25 MAY 2002	0.457	
		23 JUL 2002		0.488
7	EARTH	16 APR 2003	0.000	0.132
	DSM	18 MAY 2003	0.164	
8	MARS	12 SEP 2003	0.000	0.001
	DSM	9 AUG 2004	0.577	
		15 JUL 2004		0.619

continued

Table 4.2 Concluded

			BPLANE	PRIMER
LEG NUMBER	SWINGBY PLANET	DATE	ΔV (KM/SEC)	ΔV (KM/SEC)
9	EARTH	7 JUL 2005	0.000	0.042
	DSM	5 AUG 2005	0.225	
10	MARS	13 DEC 2005	0.000	0.002
	DSM	17 OCT 2006	0.370	
		27 JUL 2006		0.419
11	EARTH	6 SEP 2007	0.000	0.023
	DSM	30 SEP 2007	0.188	
12	MARS	16 FEB 2008	0.000	0.001
	DSM	25 MAR 2009	0.071	
		15 FEB 2009		0.075
13	EARTH	10 OCT 2009	0.000	0.009
	DSM	7 NOV 2009	0.012	
14	MARS	28 MAR 2010	0.000	0.003
	DSM	14 MAY 2011	0.079	
		11 MAR 2011		0.069
	EARTH	13 NOV 2011	0.039	0.048

TOTAL ΔV (KM/SEC)	4.533	2.212
RUN TIME (SEC)	332.2	54.6

Table 4.3: Vehicle and Mission Parameters for Round Trip Mars Mission Launch Window Analysis

Vehicle

Mars drop off mass, kg	76000
Earth return mass, kg	61000
Engine Specific Impulse (Isp), sec	480

Mission

Earth departure parking orbit	500 km altitude, circular
Mars parking orbit	500 km periapsis altitude, 1 sol
Earth return parking orbit	500 km periapsis altitude, 1 sol
Outbound time of flight	108 to 418 days
Mars stay time	60 days
Inbound time of flight	73 to 383 days
Maximum total time of flight	730 days

Table 4.4: Vehicle and Mission Parameters for Nominal Mars Mission Abort Analysis

Vehicle

Mars drop off mass, kg76000
 Earth return mass, kg61000
 Engine Specific Impulse (Isp), sec475

Mission

Earth departure parking orbit500 km altitude, circular
 Mars parking orbit500 km periapsis altitude, 1 sol
 Earth return parking orbit500 km periapsis altitude, 1 sol

Dates

	2020 Mission	2022 Mission
Launch Date	11 Sep. 2020	11 Oct. 2022
Outbound time of flight	278 days	288 days
Mars stay time	60 days	60 days
Inbound time of flight	383 days	383 days
Total time of flight	721 days	731 days

Table 4.5.1 Comparison Between Nominal and Abort Trajectories for 2020 Mars Mission

	Nominal	Abort Without DSM	Abort With DSM
Initial Mass (million kg)	1.6	9.9	4.1
Total ΔV (km/sec)	14.5	23.6	19.4
Time of flight (days)	721	651	501

Table 4.5.2 Comparison Between Nominal and Abort Trajectories for 2022 Mars Mission

	Nominal	Abort Without DSM	Abort With DSM
Initial Mass (million kg)	2.7	4.5	3.8
Total ΔV (km/sec)	15.0	19.8	18.9
Time of flight (days)	731	681	511

9. Figures

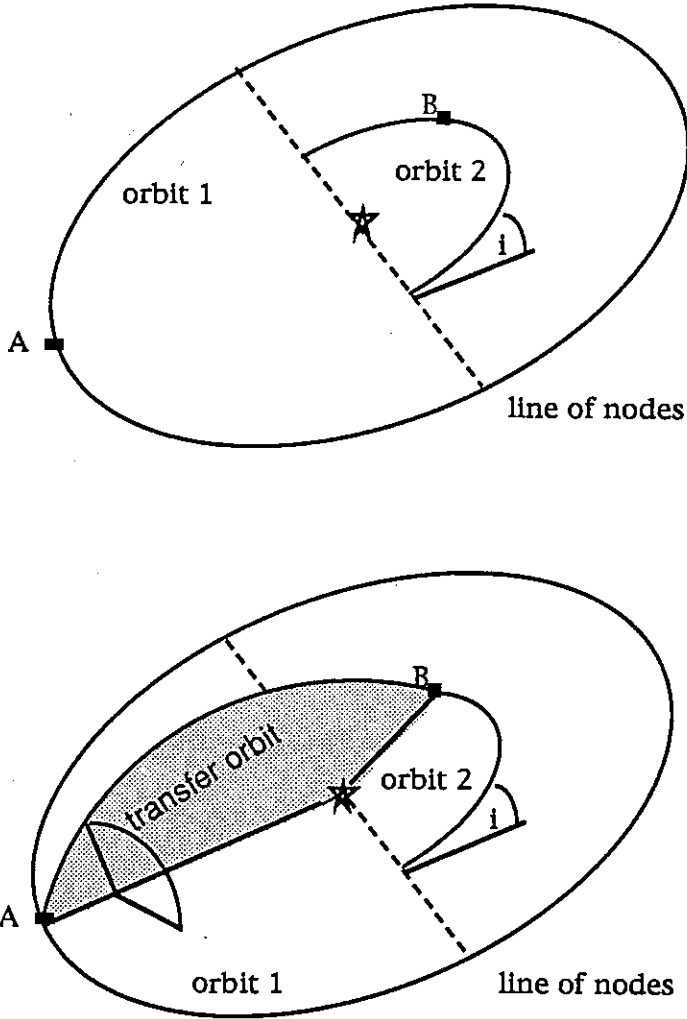


Figure 1.1: Rendezvous Between Points A and B

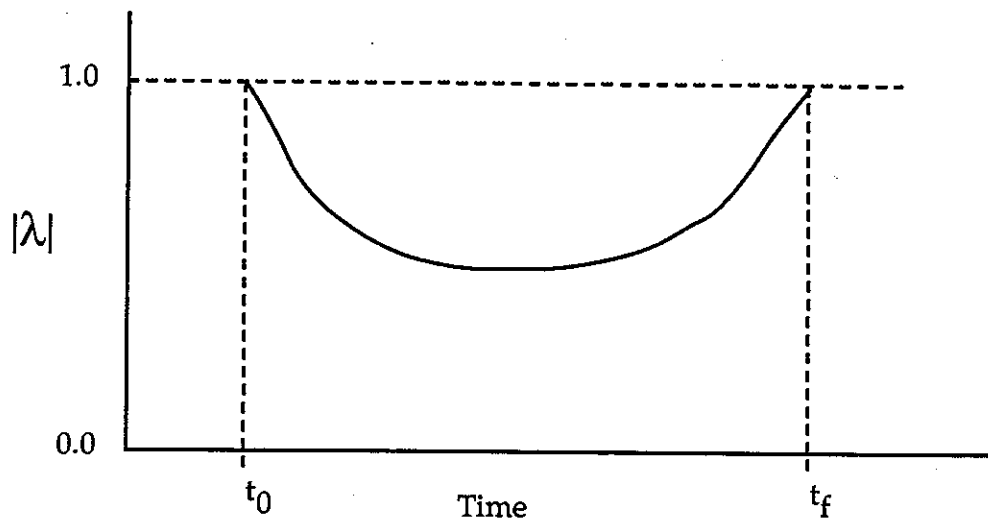


Figure 1.2: Representative Optimal Primer Magnitude History

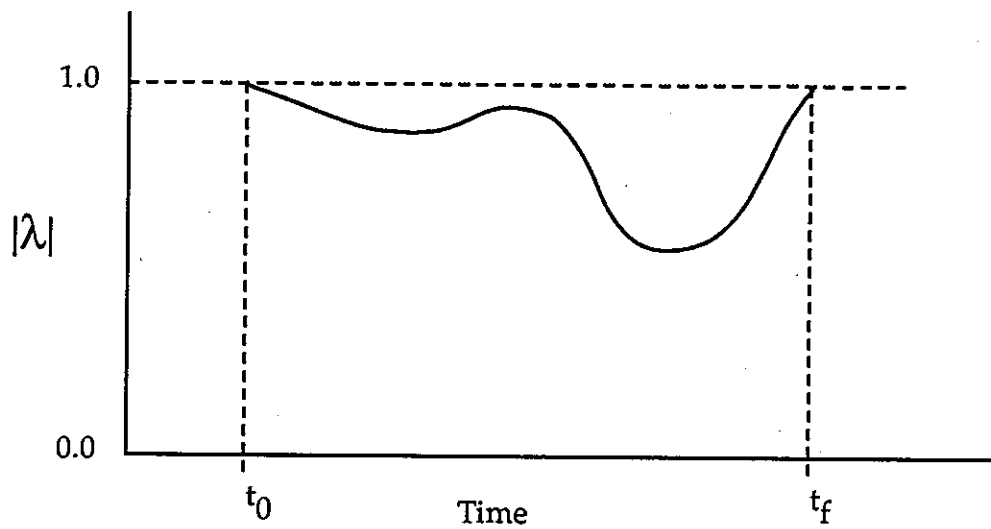


Figure 1.3: Representative Optimal Primer Magnitude History

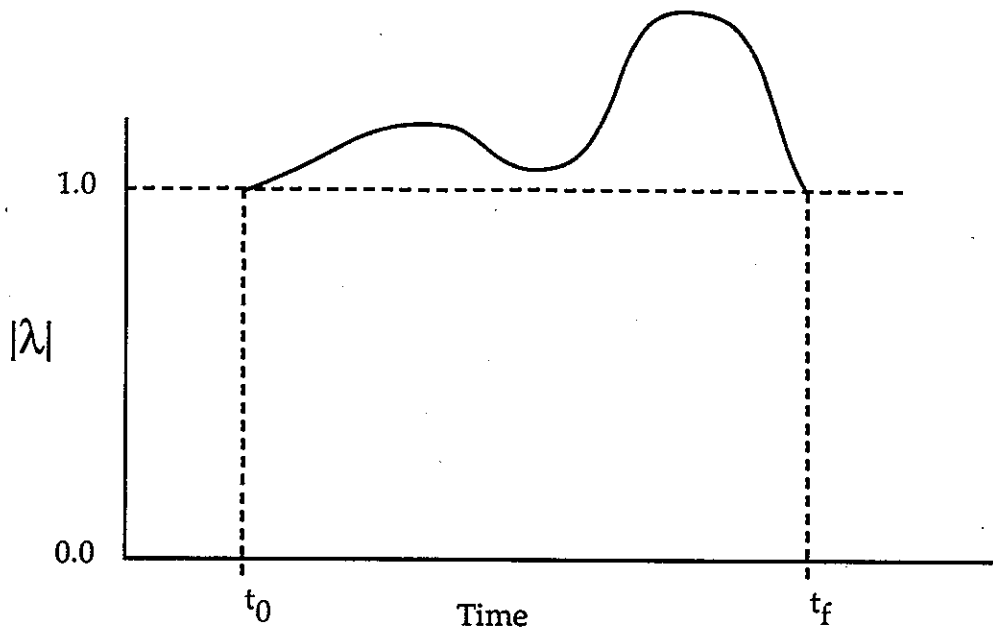


Figure 1.4: Representative Non-Optimal Primer Magnitude History

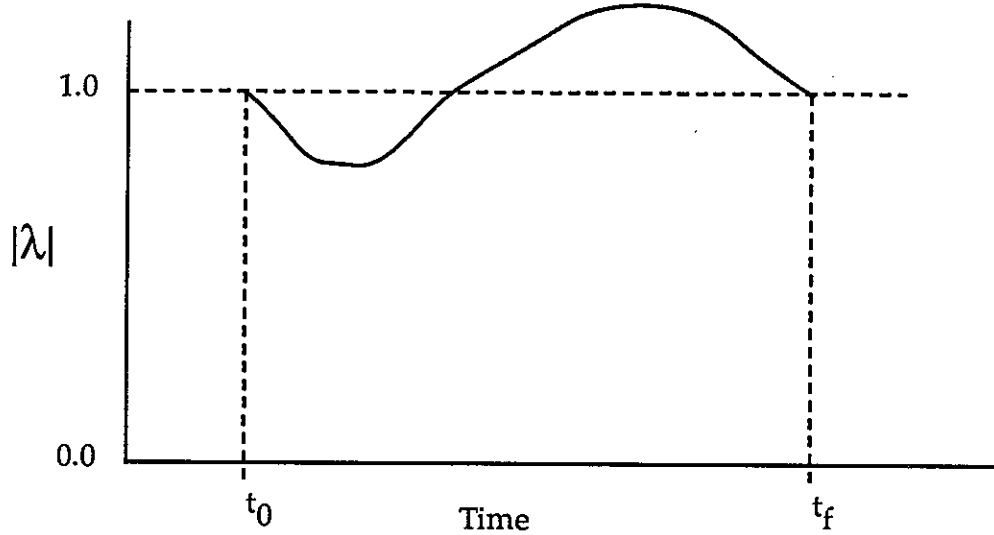


Figure 1.5: Representative Non-Optimal Primer Magnitude History

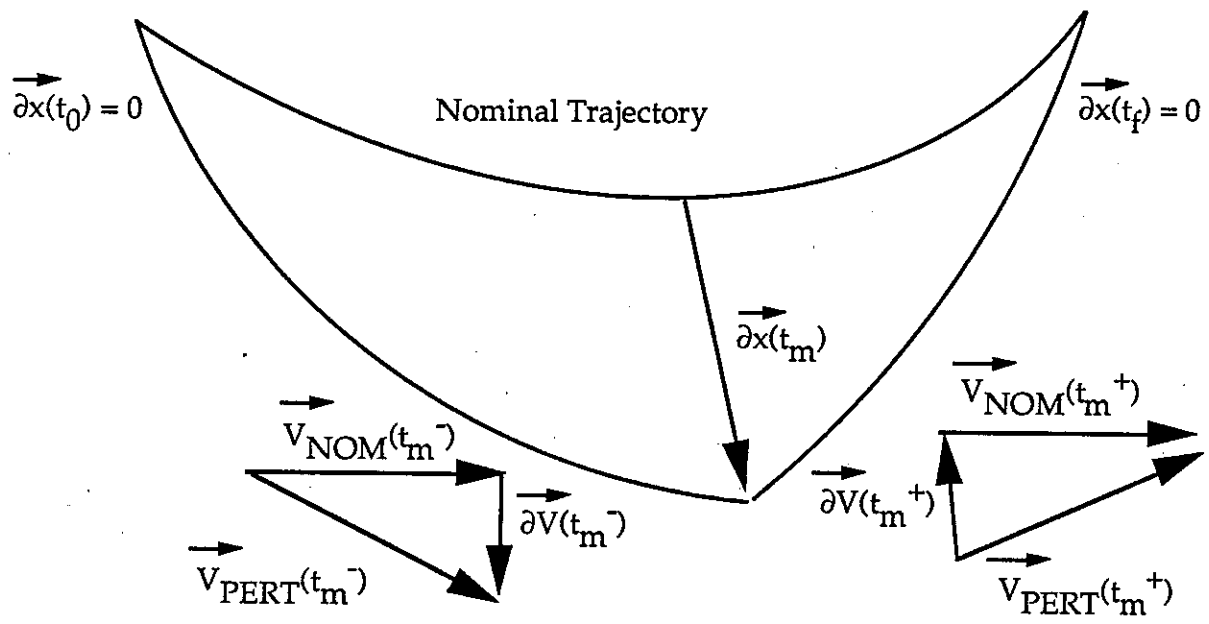


Figure 2.1: Perturbations from the Nominal Trajectory

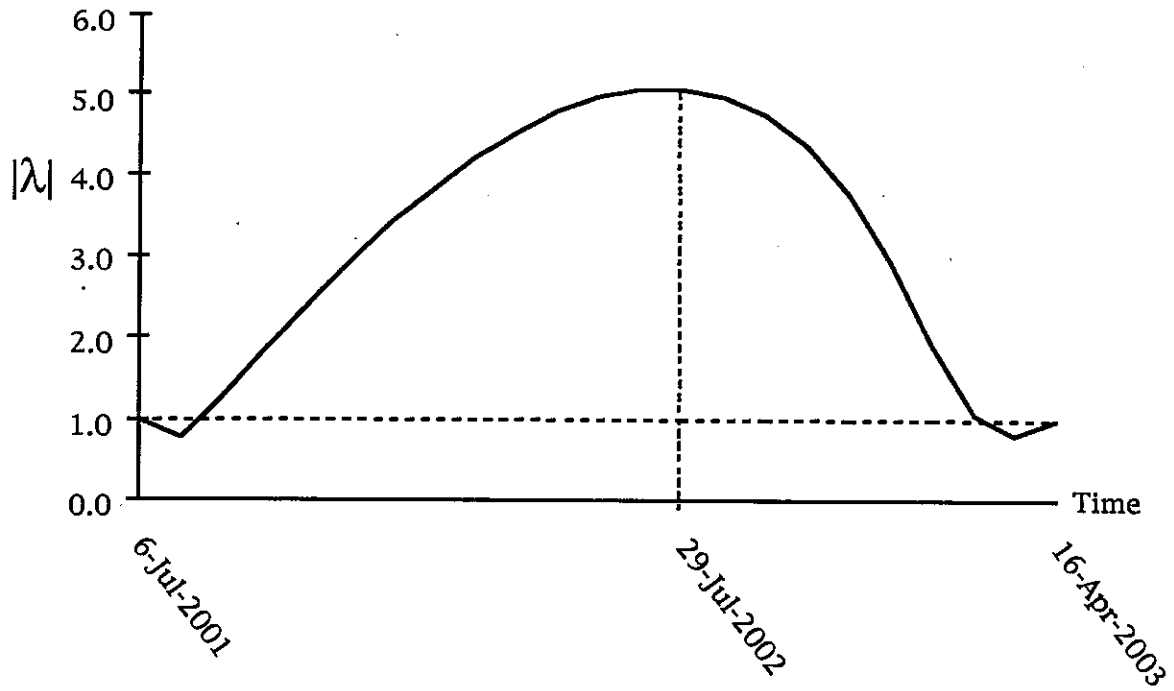


Figure 4.1: Primer Magnitude History for Leg 6 in Table 4.1

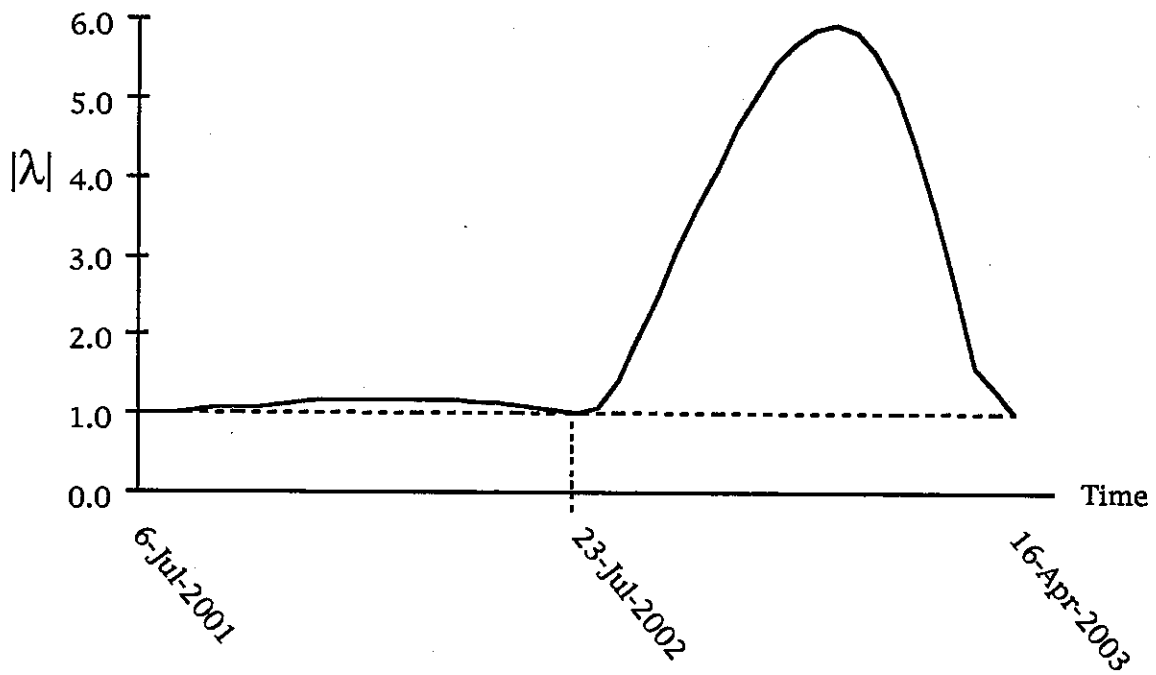


Figure 4.2: Primer Magnitude History for Leg 6 With DSM

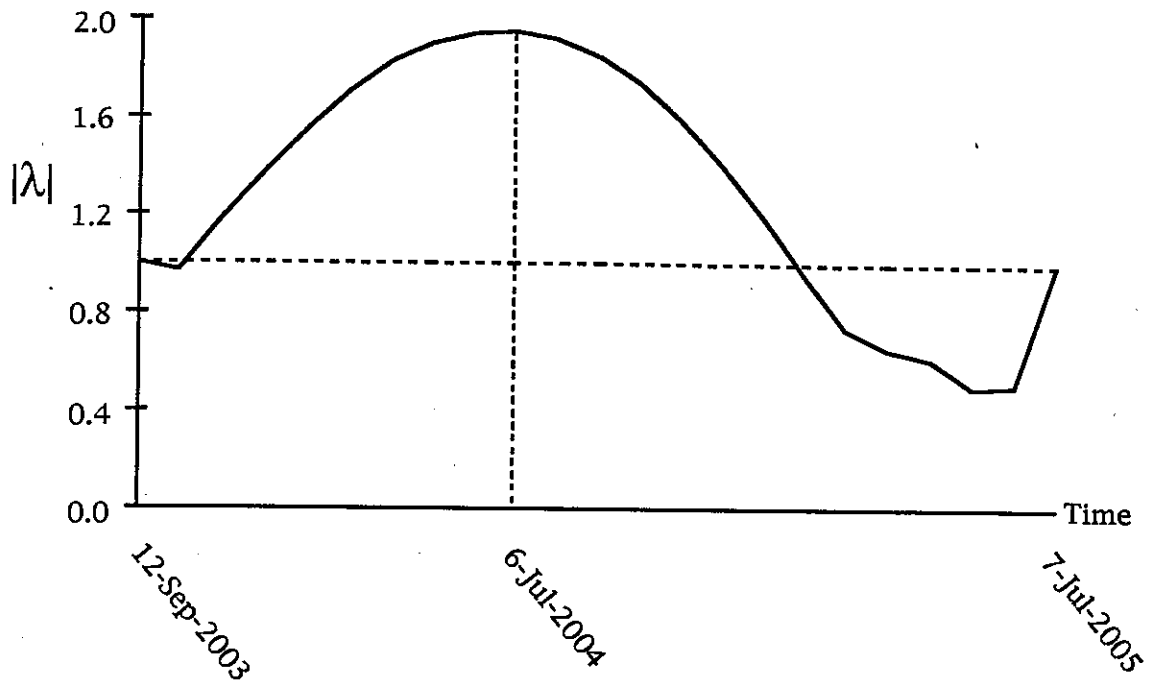


Figure 4.3: Primer Magnitude History for Leg 8 in Table 4.1

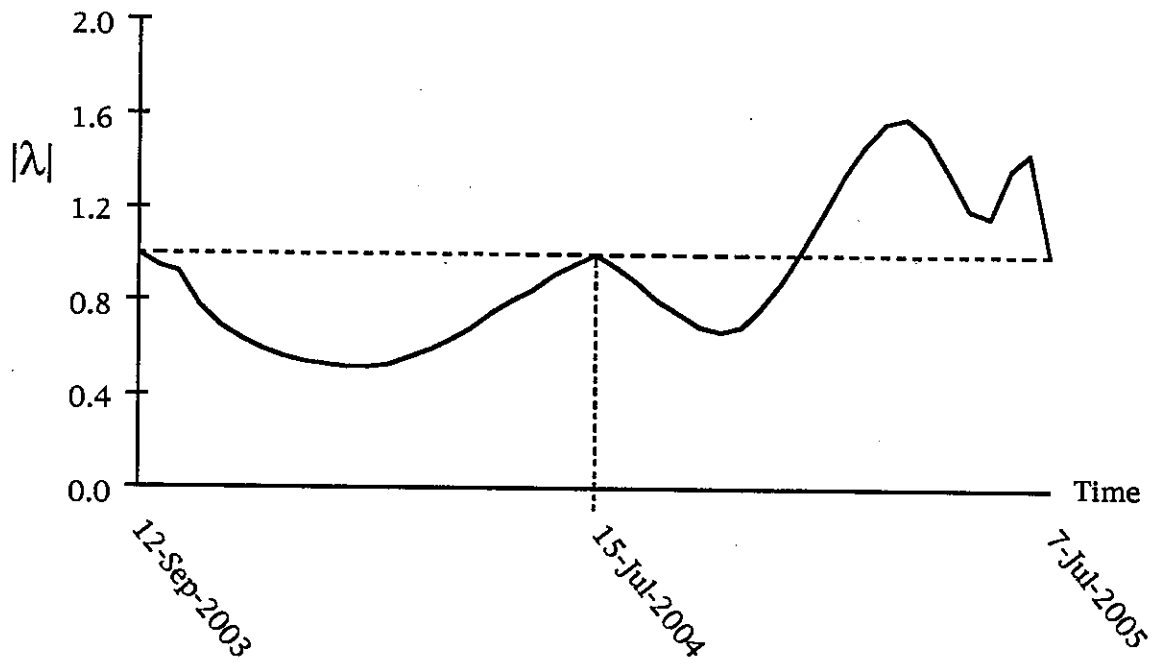


Figure 4.4: Primer Magnitude History for Leg 8 With DSM

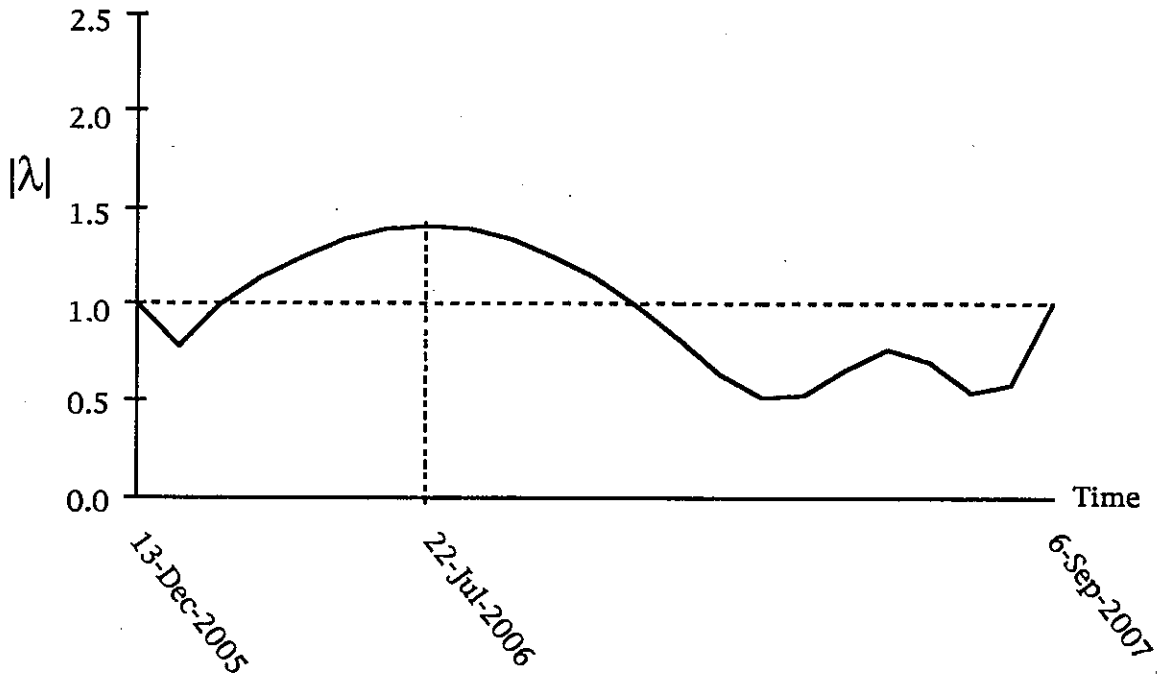


Figure 4.5: Primer Magnitude History for Leg 10 in Table 4.1

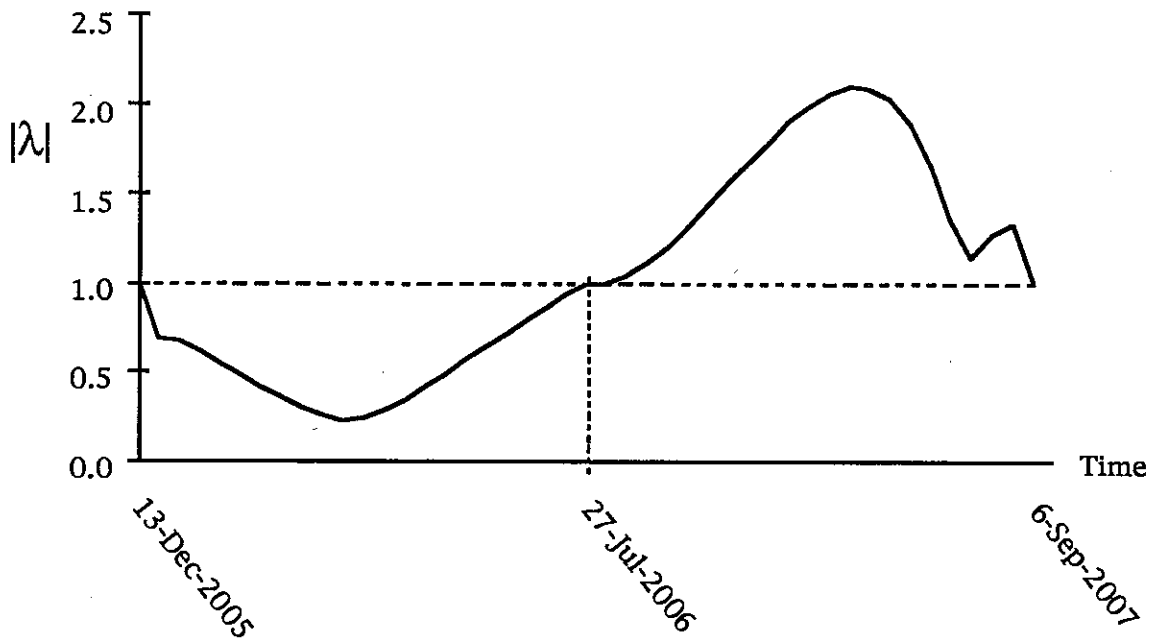


Figure 4.6: Primer Magnitude History for Leg 10 With DSM

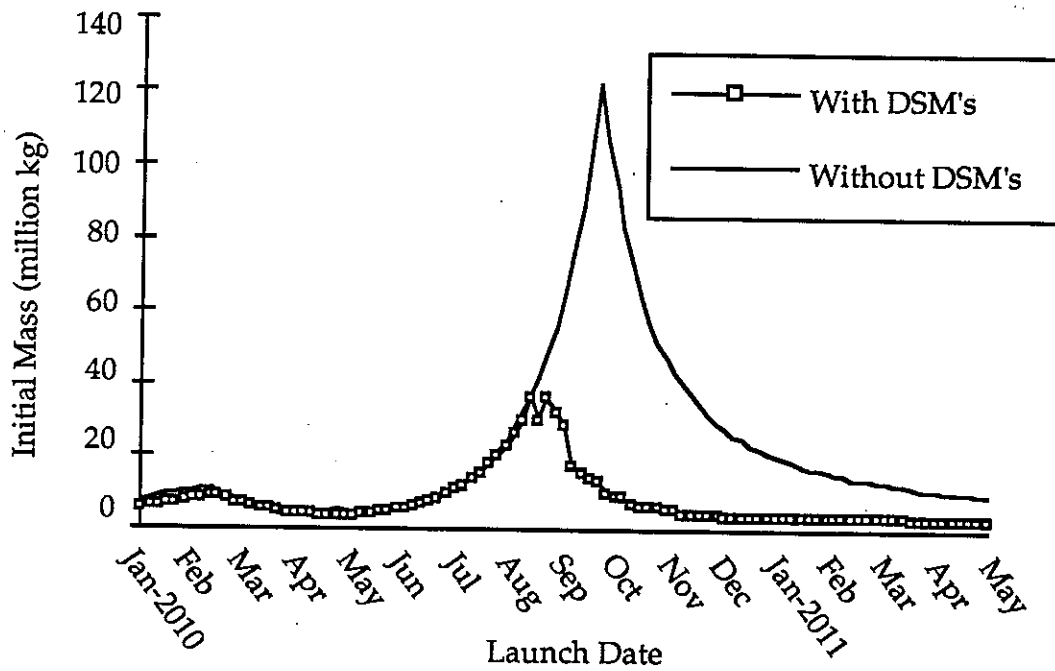


Figure 4.7.1: Initial Mass vs Launch Date for Round Trip Mars Mission

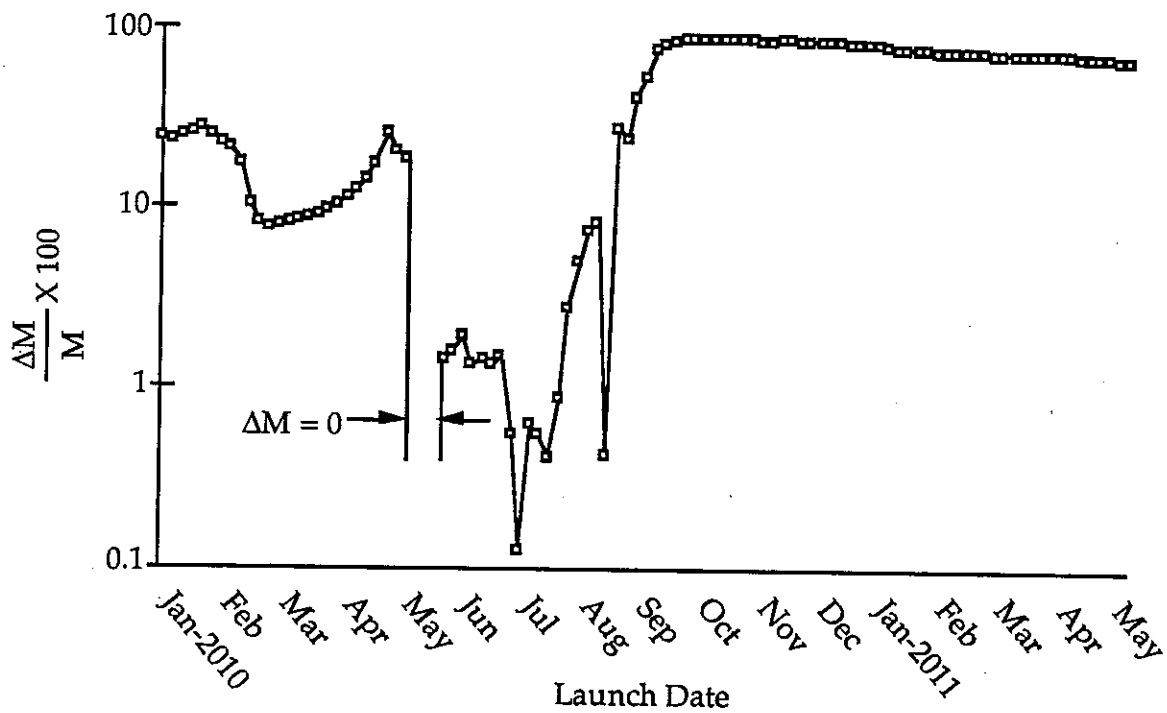


Figure 4.7.2: Percent Savings of Initial Mass

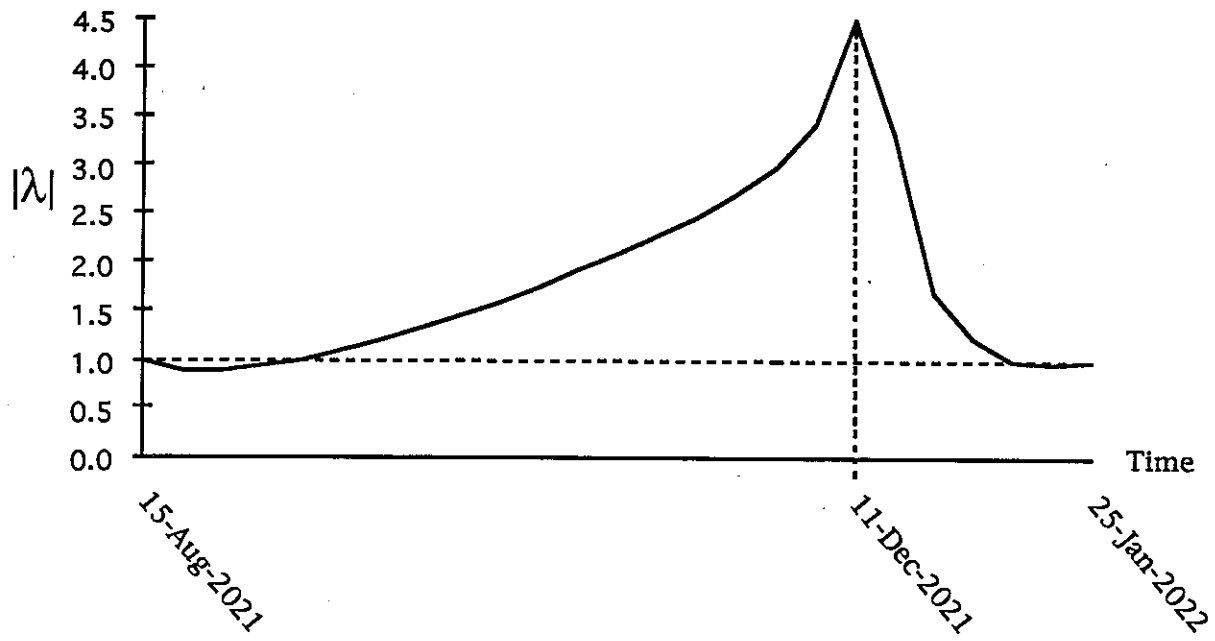


Figure 4.8: Primer Magnitude History for 2020 Abort Mission

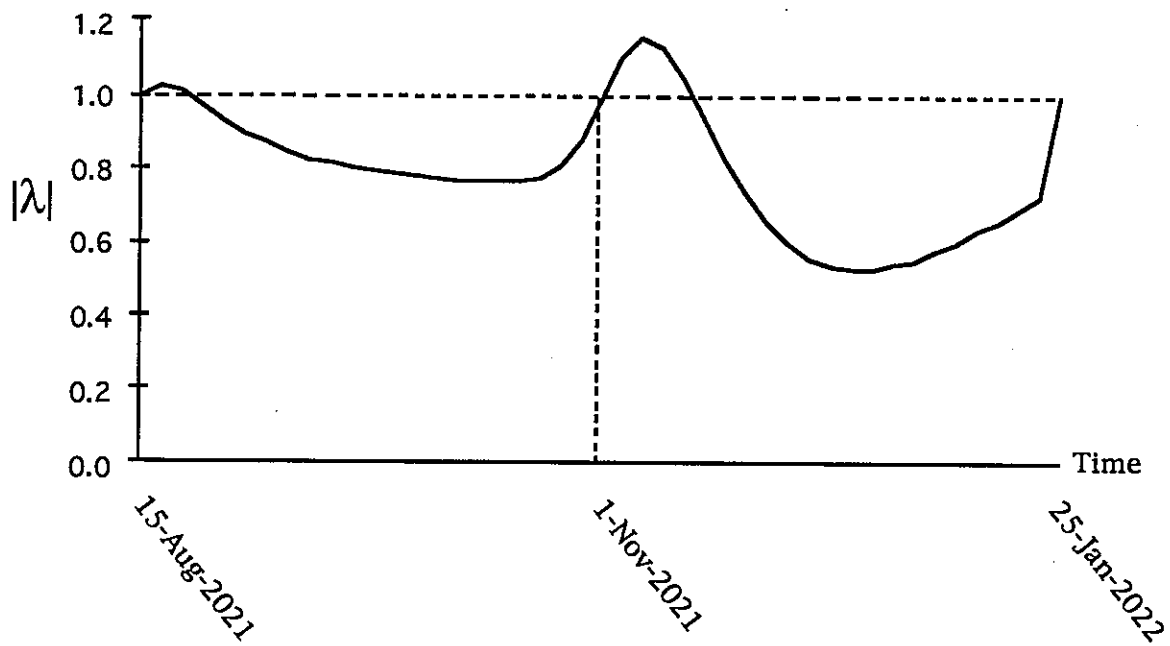


Figure 4.9: Primer Magnitude History for 2020 Abort Mission With DSM

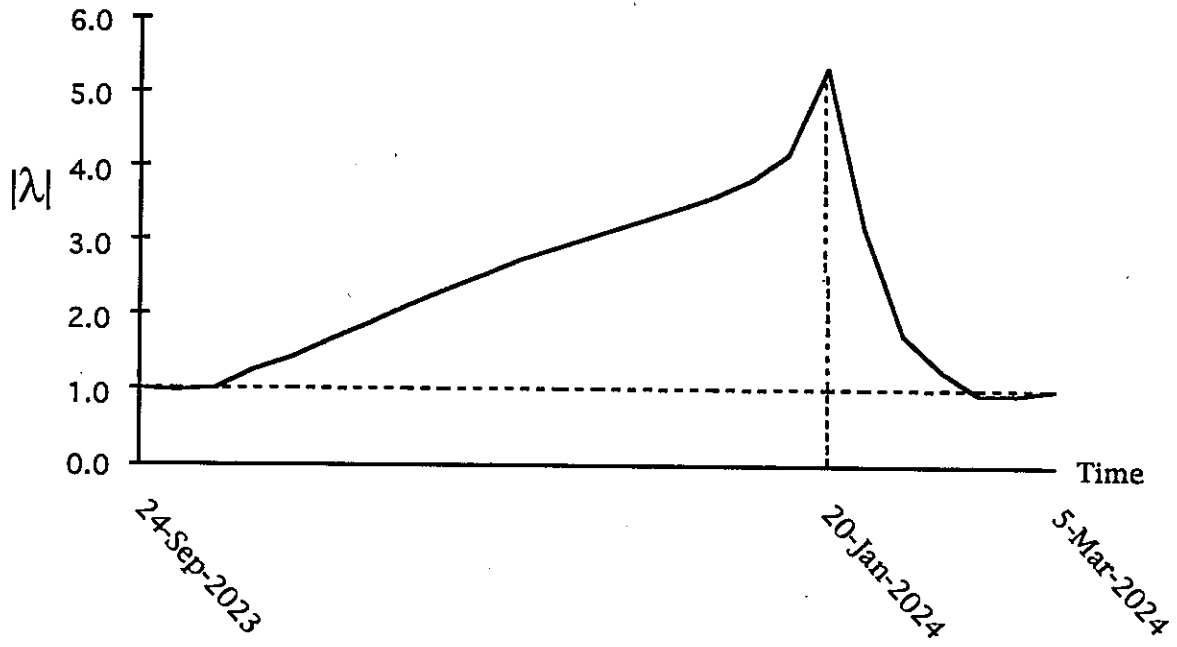


Figure 4.10: Primer Magnitude History for 2022 Abort Mission

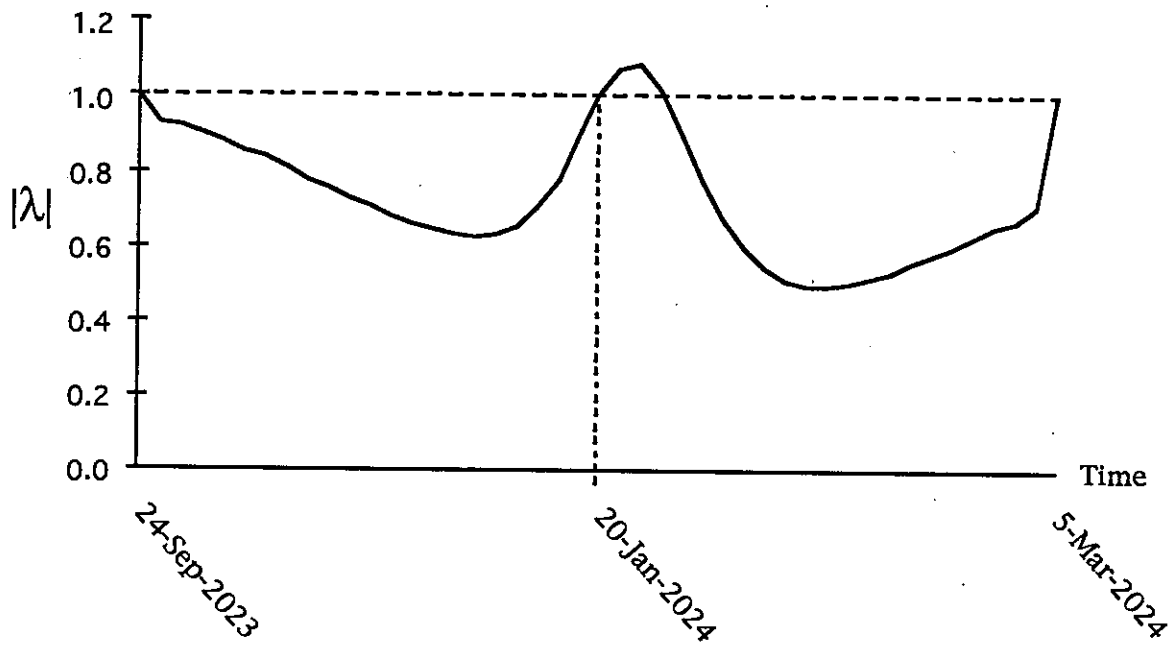


Figure 4.11: Primer Magnitude History for 2022 Abort Mission With DSM

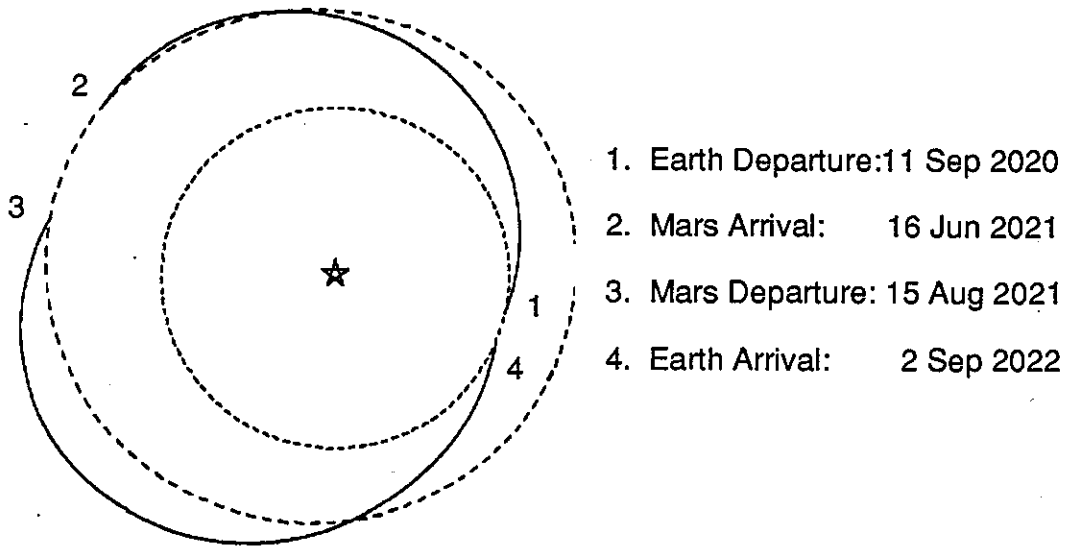


Figure 4.12: 2020 Round Trip Mars Mission

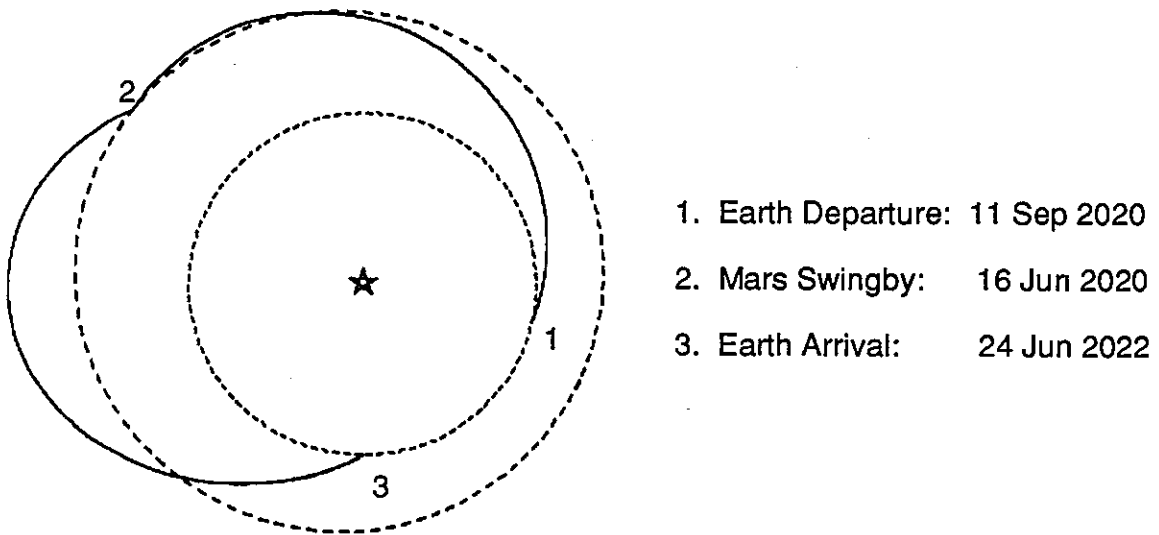
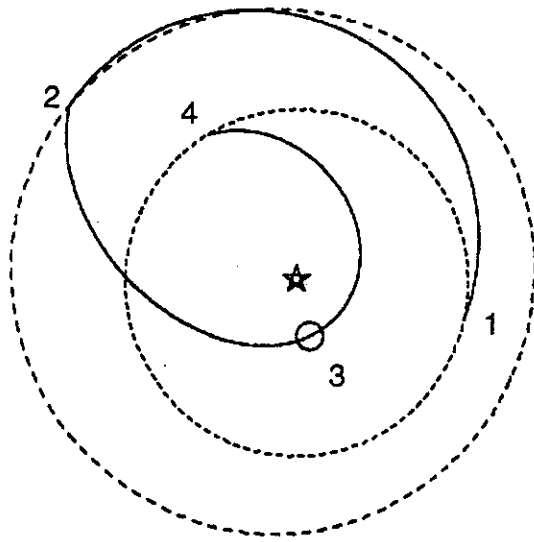
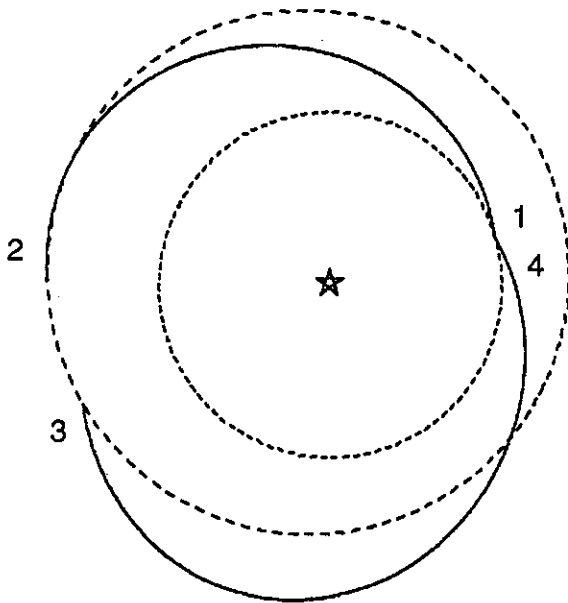


Figure 4.13: 2020 Abort Mars Mission Without DSM



- 1. Earth Departure: 11 Sep 2020
- 2. Mars Arrival: 16 Jun 2021
- 3. DSM : 1 Nov 2021
- 4. Earth Arrival: 25 Jan 2022

Figure 4.14: 2020 Abort Mars Mission With DSM



- 1. Earth Departure: 11 Oct 2022
- 2. Mars Arrival: 26 Jul 2023
- 3. Mars Departure: 24 Sep 2023
- 4. Earth Arrival: 11 Oct 2024

Figure 4.15: 2022 Round Trip Mars Mission

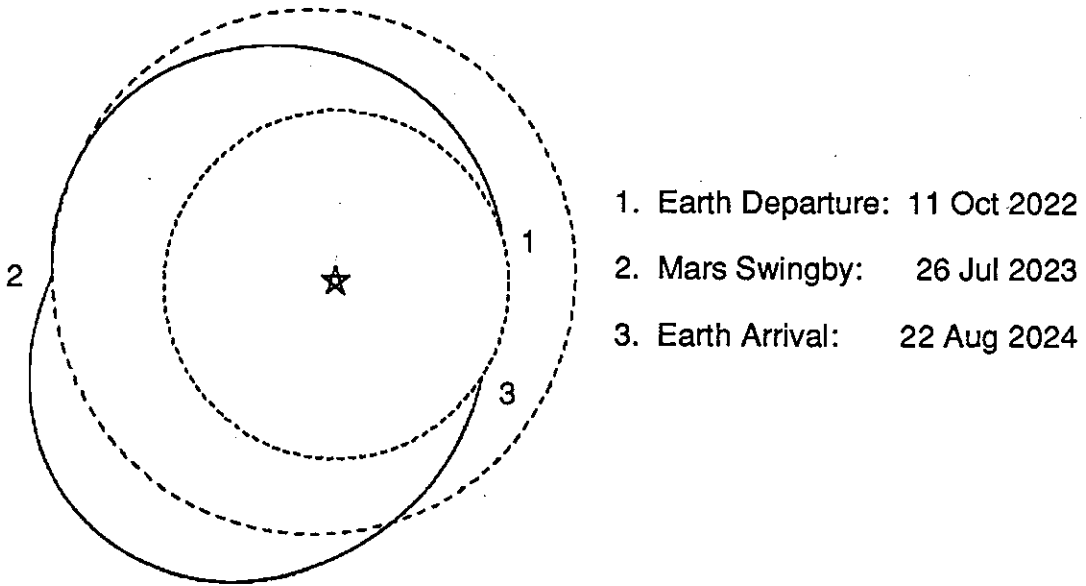


Figure 4.16: 2022 Abort Mars Mission Without DSM

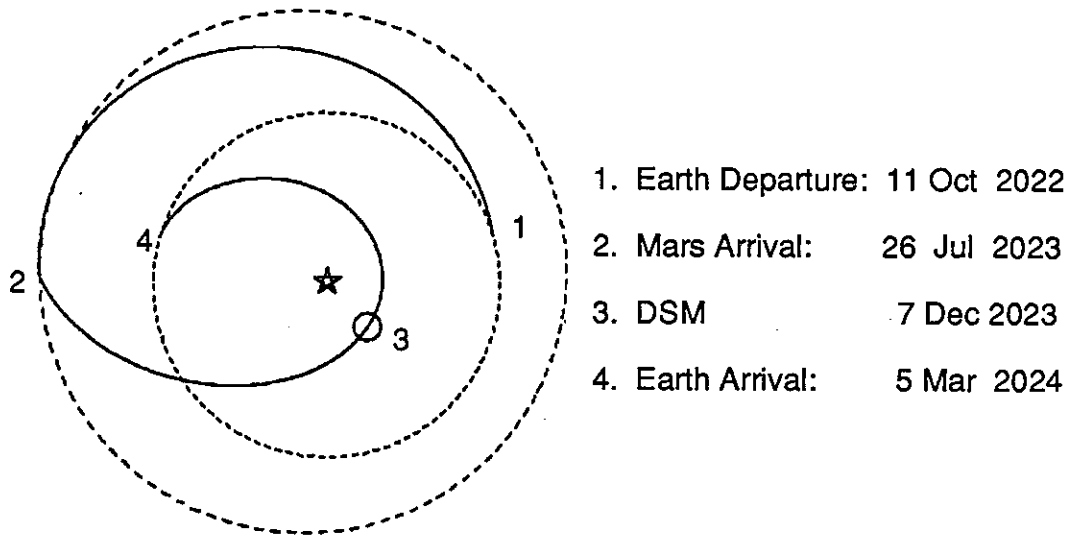


Figure 4.17: 2022 Abort Mars Mission With DSM

10. Appendix

Derivation of the Necessary Conditions on the Primer Vector

The derivation presented here is a summary of the original derivation done by D.F. Lawden². The necessary conditions on the primer vector provide the basis for this paper, and an understanding of the derivation will give the reader a stronger grasp of the subject. Indicial notation is used in this appendix. A subscript which appears only once in any term is known as a 'free index', and can take on any value in its range. A subscript which appears twice in a term is known as a 'dummy index'. A dummy index implies a summation of all terms over the range of the index.

Define a cost function, $J(x_1, x_2, \dots, x_n, t_f)$, where \bar{x} is an n-dimensional state vector. The problem is to minimize J, subject to:

$$\dot{x}_i = f_i(\bar{x}, \bar{a}, t) \text{ for } i = 1 \text{ to } n, \quad (\text{A.1})$$

$$h_k(\bar{x}, \bar{a}, t) = 0 \text{ for } k = 1 \text{ to } p < m. \quad (\text{A.2})$$

$$x_i = x_{i0} \text{ for } i = 1 \text{ to } n \text{ at time} = t_0 \quad (\text{A.3})$$

$$x_w = x_{wf} \text{ for } w = 1 \text{ to } q < n \text{ at time} = t_f \quad (\text{A.4})$$

Here, f_i are the equations of motion, h_k are constraint functions, t is time, and \bar{a} is an m-dimensional control vector. Let $\bar{x}^*(t)$ and $\bar{a}^*(t)$ be the state and control histories which satisfy the equations A.1 to A.4 and also minimize J. Introduce a small parameter ϵ , and use it to perturb these state and control vectors. That is, let

$$\bar{x}(t, \epsilon) = \bar{x}^*(t) + \epsilon(t) \text{ and } \bar{a}(t, \epsilon) = \bar{a}^*(t) + \epsilon(t).$$

Differentiate equation A.1 with respect to ϵ to obtain

$$\frac{\partial^2 x_i}{\partial \varepsilon \partial t} = \frac{\partial f_i}{\partial x_r} \frac{\partial x_r}{\partial \varepsilon} + \frac{\partial f_i}{\partial a_j} \frac{\partial a_j}{\partial \varepsilon} \quad (\text{A.5})$$

Now, let

$$y_i(t) = \left(\frac{\partial x_i}{\partial \varepsilon} \right)_{\varepsilon=0}$$

and

$$\beta_j(t) = \left(\frac{\partial a_j}{\partial \varepsilon} \right)_{\varepsilon=0}$$

so at $\varepsilon = 0$, equation A.5 becomes

$$\dot{y}_i = \frac{\partial f_i}{\partial x_r} y_r + \frac{\partial f_i}{\partial a_j} \beta_j \quad (\text{A.6})$$

Similarly, by taking the derivative of equation A.2 with respect to ε :

$$\frac{\partial h_k}{\partial x_i} y_i + \frac{\partial h_k}{\partial a_j} \beta_j = 0 \quad (\text{A.7})$$

Now the Lagrange expression is introduced:

$$F = -\lambda_i f_i + \mu_k h_k \quad (\text{A.8})$$

This is where the primer vector is introduced. The primer vector is a Lagrange multiplier. In problems of the type being considered here, the state vector is a 7-dimensional vector, with the first three components being the velocity of a spacecraft, the next three components being the position of the spacecraft, and the last component being the mass of the spacecraft. The components of the primer vector are, by definition, the first three components of $\vec{\lambda}$. It will be shown that the derivative of the primer vector is a vector whose components are the next three components of $\vec{\lambda}$.

From the definition of F:

$$\int_{t_0}^{t_f} \left(\lambda_i \dot{y}_i + \frac{\partial F}{\partial x_i} y_i + \frac{\partial F}{\partial a_j} \beta_j \right) dt = \int_{t_0}^{t_f} \left(\lambda_i \left(\dot{y}_i - \frac{\partial f_i}{\partial x_r} y_r - \frac{\partial f_i}{\partial a_j} \beta_j \right) + \mu_k \left(\frac{\partial h_k}{\partial x_r} y_r + \frac{\partial h_k}{\partial a_j} \beta_j \right) \right) dt \quad (\text{A.9})$$

By equations A.6 and A.7, this expression equals 0 on an optimal trajectory.

Integration by parts yields:

$$\int_{t_0}^{t_f} \frac{\partial F}{\partial x_i} y_i dt = y_i G_i \Big|_{t_0}^{t_f} - \int_{t_0}^{t_f} \dot{y}_i G_i dt$$

where

$$G_i = \int \frac{\partial F}{\partial x_i} dt$$

The parameters λ_i and μ_k are at our disposal, and so λ_i can be chosen such that

$$\lambda_i = G_i + \lambda_{i0} \quad (\text{A.10})$$

where λ_{i0} are constants yet to be determined, and μ_k can be chosen such that

$\frac{\partial F}{\partial a_k} = 0$. Equation A.10 can also be expressed as $\lambda_i = \frac{\partial F}{\partial x_i}$. Equation A.9 can now be

reduced to

$$0 = y_{if} \lambda_{if} - y_{i0} \lambda_{i0} + \int_{t_0}^{t_f} \frac{\partial F}{\partial a_r} \beta_r dt \quad (\text{A.11})$$

where $r = p+1, p+2, \dots, m$ and $\lambda_{if} = \lambda_i(t_f)$. This result will be used later.

Define a family of variations ϵ^σ , where σ runs from 1 to N , and $N = q + n + 1$. Each member of this family satisfies equations A.1 to A.4. Now J can be expressed as a function of these variations:

$$J = J(\epsilon^1, \epsilon^2, \dots, \epsilon^N) = J_0 + U$$

where J_0 is the minimum J . $U = 0$ if and only if $\epsilon^\sigma = 0$ for all σ . In all other cases, U must be positive, since J_0 is by definition the minimum J . Theory of implicit

functions tells us that ϵ^σ can be determined as a continuous function of U in the neighborhood of U=0 if and only if the determinant

$$\Delta = \begin{vmatrix} \frac{\partial J}{\partial \epsilon^1} & \frac{\partial J}{\partial \epsilon^2} & \dots & \frac{\partial J}{\partial \epsilon^N} \\ \frac{\partial x_{i0}}{\partial \epsilon^1} & \frac{\partial x_{i0}}{\partial \epsilon^2} & \dots & \frac{\partial x_{i0}}{\partial \epsilon^N} \\ \frac{\partial x_{wf}}{\partial \epsilon^1} & \frac{\partial x_{wf}}{\partial \epsilon^2} & \dots & \frac{\partial x_{wf}}{\partial \epsilon^N} \end{vmatrix}$$

is not zero. If the determinant is not zero, it implies that there are some variations which produce a negative value of U. This cannot be the case, since U must be greater than or equal to zero. The conclusion is that the determinant must vanish, and therefore that the rows of the above matrix must be linearly dependent. This means that N constants γ_0, γ_i ($i = 1$ to n), and v_w ($w = 1$ to q) can be found such that

$$\gamma_0 \frac{\partial J}{\partial \epsilon^z} + \gamma_i \frac{\partial x_{i0}}{\partial \epsilon^z} + v_1 \frac{\partial x_{wf}}{\partial \epsilon^z} = 0 \quad (\text{A.12})$$

for arbitrary z in the range of 1 to N. Looking at each of the three terms in this equation when $\epsilon^z = 0$ (optimal trajectory):

$$\left(\frac{\partial J}{\partial \epsilon^z} \right)_{\epsilon^z=0} = \frac{\partial J}{\partial x_{sf}} \left(\frac{\partial x_s}{\partial t_f} u_f^z + \frac{\partial x_s}{\partial \epsilon^z} \right) + \frac{\partial J}{\partial t_f} u_f^z$$

where

$$s = q+1, q+2, \dots, n$$

$$x_s = \text{free states at } t = t_f$$

$$u_f^z = \left(\frac{dt_f}{d\epsilon^z} \right)_{\epsilon^z=0}$$

The second and third terms become:

$$\frac{\partial x_{i0}}{\partial e^z} = y_{i0}$$

$$\frac{\partial x_{wf}}{\partial e^z} = \dot{x}_{wf} u_f^z + y_{wf} \quad (\text{no sum over } f)$$

Inserting these three expressions into A.12, and also adding in equation A.11:

$$0 = (\gamma_i - \lambda_{i0})y_{i0} + (v_w + \lambda_{wf})y_{wf} + \left(\gamma_0 \frac{\partial J}{\partial x_{sf}} + \lambda_{sf} \right) y_{sf} + \left(\gamma_0 \frac{\partial J}{\partial x_{sf}} \dot{x}_{sf} + \gamma_0 \frac{\partial J}{\partial t_f} + v_w \dot{x}_{wf} \right) u_f^z + \int_{t_0}^{t_f} \frac{\partial F}{\partial a_r} \beta_r dt \quad (\text{A.13})$$

The ranges of the indices in equation A.13 are as follows:

$$i = 1 \text{ to } n \quad (n = \text{number of states})$$

$$w = 1 \text{ to } q \quad (q = \text{number of fixed final states})$$

$$s = (q+1) \text{ to } n$$

$$r = (p+1) \text{ to } m \quad (p = \text{number of constraints}, m = \text{number of controls})$$

The subscripts 0 and f indicate initial and final conditions, and are not indices to be summed over.

In order for equation (A.13) to vanish for arbitrary variations, each of the terms must vanish:

$$\lambda_{i0} = \gamma_i \quad (\text{A.14})$$

$$v_w = -\lambda_{wf} \quad (\text{A.15})$$

$$\gamma_0 \frac{\partial J}{\partial x_{sf}} = -\lambda_{sf} \quad (\text{A.16})$$

$$\gamma_0 \frac{\partial J}{\partial t_f} + \gamma_0 \frac{\partial J}{\partial x_{sf}} \dot{x}_{sf} + v_w \dot{x}_{wf} = 0 \quad (\text{A.17})$$

$$\frac{\partial F}{\partial a_r} = 0 \quad (\text{A.18})$$

Substituting (A.15) and (A.16) into (A.17), and realizing that

$$\lambda_{sf}\dot{x}_{sf} + \lambda_{wf}\dot{x}_{wf} = \lambda_{if}\dot{x}_{if}$$

the result is

$$\lambda_{if}\dot{x}_{if} = \gamma_0 \frac{\partial J}{\partial t_f} \quad (\text{A.19})$$

These equations are now ready to be solved. There are $2n + m + p$ unknown functions which are the n state variables x_i , the m control variables a_j , the n functions λ_i , and the p functions μ_k . We have the same number of equations in (A.1: n equations), (A.2: p equations), (A.10: n equations), and (A.18: m equations). We also have the n equations A.3, q equations A.4, $(n-q)$ equations A.16, and 1 equation A.19 to determine the n constants λ_{i0} , the n constants of integration for the state variables, and t_f . If t_f is fixed for a particular problem, equation A.19 no longer applies. If these necessary conditions can be satisfied for $\gamma_0 \neq 0$, then the solution is said to be *normal* and γ_0 can be chosen to equal 1 in equation A.12 without loss of generality.

Examine a trajectory problem defined as follows:

$$\dot{v}_i = \frac{cm}{M} l_i + g_i$$

$$\dot{r}_i = v_i$$

$$\dot{M} = -m$$

where $i = 1,2,3$ for the X,Y, and Z coordinates, $\frac{cm}{M}$ is the magnitude of the engine thrust per unit mass, l_i are the direction cosines of the thrust vector, and g_i are the

components of gravitational acceleration. M is the mass of the spacecraft and m is the propellant mass flow rate. Two constraint equations can be defined:

$$l_1^2 + l_2^2 + l_3^2 = 1$$

$$m(m_{\max} - m) = 0$$

The latter equation indicates that only no-thrust or maximum-thrust arcs are allowed on this trajectory. The state vector is:

$$[v_1 \ v_2 \ v_3 \ r_1 \ r_2 \ r_3 \ M]^T$$

and the control vector is:

$$[l_1 \ l_2 \ l_3 \ m]^T$$

The Lagrange expression is:

$$F = -\lambda_i \left(\frac{cm}{M} l_i + g_i \right) - \lambda_{i+3} v_i + \lambda_7 m + \mu_1 (l_1^2 + l_2^2 + l_3^2 - 1) + \mu_2 [m(m_{\max} - m)]$$

Employing equation A.18 and the derivative of A.10 yields:

$$\dot{\lambda}_i = -\lambda_{i+3} \quad (\text{A.20})$$

$$\dot{\lambda}_{i+3} = -\lambda_j \frac{\partial g_j}{\partial r_i} \quad (\text{A.21})$$

$$\dot{\lambda}_7 = \frac{cm}{M^2} \lambda_i l_i \quad (\text{A.22})$$

$$0 = -\frac{cm}{M} \lambda_i + 2\mu_1 l_i \quad (\text{A.23})$$

$$0 = -\frac{c}{M} \lambda_i l_i + \lambda_7 + \mu_2 (m_{\max} - 2m) \quad (\text{A.24})$$

for i and $j = 1$ to 3 . The first two of these equation can be combined to form:

$$\ddot{\lambda}_i = \lambda_j \frac{\partial g_j}{\partial r_i}$$

Equations A.20 and A.21 indicate that the primer and its derivative are continuous functions of time.

The Weierstrass condition² (submitted here without proof) for this problem can be expressed as:

$$\left(\frac{c}{M} \lambda_i l_i - \lambda_7 \right) m \geq \left(\frac{c}{M} \lambda_i l_i^* - \lambda_7 \right) m^*$$

for all possible values of l^* and m^* which satisfy the constraints. On a no-thrust arc, $m=0$, and so the condition requires that the right hand side be negative, or that:

$$\lambda_7 \geq \frac{c}{M} \lambda_i l_i^*$$

The right hand side of this expression takes its maximum value when the primer is aligned with the thrust vector. Thus, the condition on no-thrust arcs becomes:

$$\lambda_7 \geq \frac{c}{M} p$$

where p is the magnitude of the primer vector.

On max-thrust arcs, two cases need to be considered. First, let m^* take on its maximum value, m_{\max} . In order for the Weierstrass condition to be satisfied:

$$\lambda_i l_i \geq \lambda_i l_i^*$$

which implies that:

$$\lambda_i l_i \geq p$$

Since \bar{l} is a unit vector, the $>$ will never hold, and so:

$$\lambda_i l_i = p$$

This indicates that the thrust vector must always be aligned with the primer vector. For the second case, let m^* take on its minimum value of 0, then it is necessary that the left hand side of the Weierstrass condition be positive:

$$\lambda_7 \leq \frac{c}{M} \lambda_i l_i \Rightarrow \lambda_7 \leq \frac{c}{M} p$$

on max-thrust arcs. This leads us to define the *switching function* κ :

$$\kappa = \frac{c}{M} p - \lambda_7$$

On no-thrust arcs, it is necessary that the switching function must be less than or equal to zero. On max-thrust arcs, the switching function must be greater than or equal to zero. If impulsive thrusts are allowed in the simulation, periods of maximum thrust are modeled to be instantaneous, and the switching function must equal zero at an impulse. If an impulse is required at a point which is not at either end of a trajectory (a deep space maneuver), the value of the switching function must be negative immediately preceding and immediately following the burn. The derivative of the switching function has been shown² to be continuous, and therefore, at a deep space maneuver, the derivative of the switching function must also be zero.

Define the cost function, J , to be the sum of the magnitudes of the ΔV 's over the whole trajectory, which, by the rocket equation, can be expressed as:

$$J = c \ln \left(\frac{M_0}{M_f} \right) = g_0 I_{sp} \ln \left(\frac{M_0}{M_f} \right)$$

With this cost function defined,

$$\lambda_7 = \frac{c}{M_f} = \frac{c}{M}$$

by equation A.16 at time = t_f . Equation A.22 shows that λ_7 is constant on a no-thrust arc (since $m=0$). Therefore, on a no-thrust arc,

$$\kappa = \frac{c}{M}p - \lambda_7 = \frac{c}{M}(p - 1) \quad (\text{A.25})$$

At the two impulses surrounding this no-thrust leg, the switching function equals zero, and so p must equal 1. Also, the switching function must never be positive on a trajectory consisting only of impulses and no-thrust arcs. So the maximum magnitude of the primer vector is unity, and that only occurs at the impulses. Equation A.25 indicates that

$$\dot{\kappa} = \frac{c}{M}\dot{p}$$

We have said that κ must be zero at a deep space maneuver, therefore, the derivative of the magnitude of the primer vector must also be zero there.

Four necessary conditions to be satisfied for an optimal trajectory allowing impulsive thrust, and whose cost function is the sum of the ΔV 's have been derived:

- 1) The primer vector and its first time derivative are continuous.
- 2) During any impulse, the thrust vector must be aligned with the primer.
- 3) The magnitude of the primer is a maximum and has a value of one during any impulse.
- 4) The derivative of the magnitude of the primer is zero at a deep space maneuver.